U.S. Department of Energy
Office of FreedomCAR and Vehicle Technologies
1000 Independence Avenue S.W.
Washington, DC 20585-0121

FY 2003

Progress Report for Automotive Propulsion Materials Program

Energy Efficiency and Renewable Energy
Office of FreedomCAR and Vehicle Technologies

Edward Wall Program Manager

December 2003

CONTENTS

1. INTRODUCTION **1**

2. POWER ELECTRONICS **7**

A. Low-Cost, High-Energy-Product Permanent Magnets 7
B. Development of Improved Powder for Bonded Permanent Magnets 13
C. Carbon Foam for Electronics Cooling 23
D. Evaporative Cooling of Power Electronics 29
E. High-Temperature Film Capacitors 35
F. Mechanical Reliability of Electronic Materials and Electronic Devices 41

3. CIDI ENGINES **47**

A. Microwave-Regenerated Diesel Particulate Filter Durability Testing 47
B. Material Support for Nonthermal Plasma Diesel Engine Exhaust Emission Control 53
C. Fabrication of Small Fuel Injector Orifices 57
D. Technology for Producing Small Holes in Advanced Materials 63
E. Electrochemical NO_x Sensor for Monitoring Diesel Emissions 69

APPENDIX A: ACRONYMS AND ABBREVIATIONS **75**

1. INTRODUCTION

Automotive Propulsion Materials R&D: Enabling Technologies to Meet FreedomCAR Program Goals

The Department of Energy's (DOE's) Office of FreedomCAR and Vehicle Technologies (OFCVT) is pleased to introduce the FY 2003 *Annual Progress Report for the Automotive Propulsion Materials Research and Development Program*. Together with DOE national laboratories and in partnership with private industry and universities across the United States, the program continues to engage in research and development (R&D) that provides enabling materials technology for fuel-efficient and environmentally friendly light-duty vehicles.

This introduction summarizes the objectives, progress, and highlights of the program in FY 2003. It also describes the technical barriers remaining and the future direction of the program. The FY 2003 annual progress reports on *Combustion and Emission Control for Advanced CIDI Engines* and *Power Electronics* provide additional information on OFCVT's R&D activities that support the development of propulsion materials technology.

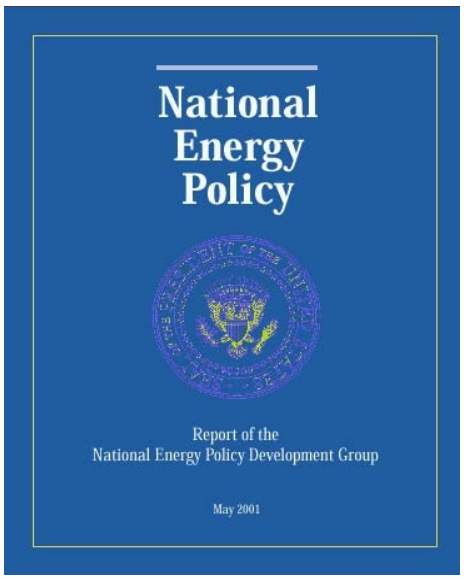

Report of the National Energy Policy Development Group

In May of 2001, the President's National Energy Policy Development Group published the National Energy Policy (NEP). This comprehensive energy policy specifically addresses the development of energy-efficient vehicle technologies, including hybrid systems, advanced emission control technologies, fuel cells, and hydrogen-based systems. The NEP is a strong indicator of the continuing federal support for advanced automotive technologies and the materials work that supports them.

The Automotive Propulsion Materials (APM) R&D Program has supported the FreedomCAR Program since its inception. FreedomCAR is not an automobile or prototype but rather a new approach to developing the technologies for vehicles of the future. In research areas where industry views the risks as too high and uncertain, the FreedomCAR Program conducts long-term research, development, and demonstration activities that bring the technology to a stage of maturity such that industry can undertake the final commercialization stages.

The APM Program is a partner with the OFCVT programs for Power Electronics and Electric Machines and for Combustion and Emissions Control for Advanced CIDI Engines. Projects within the APM Program address materials concerns that directly impact the critical technical barriers in each of these programs—barriers such as thermal management, emissions reduction, and reduced manufacturing costs. The program engages only the barriers that involve fundamental, high-risk materials issues.

Enabling Technologies

The APM Program focuses on enabling materials technologies that are critical in removing barriers to the power electronics and compression-ignition, direct-injection (CIDI) engine and emissions control research programs. The program supports these two core technology areas by providing materials expertise, testing capabilities, and technical solutions for materials problems. The component development, materials processing, and characterization that the program provides are enablers of the successful development of efficient electric drive systems and emissions-compliant CIDI engines.

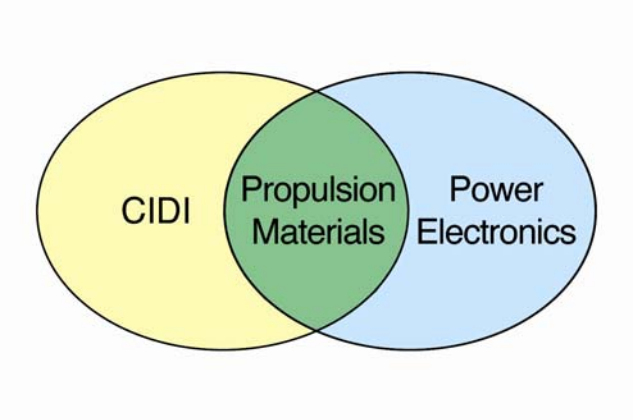

The Propulsion Materials Program focuses on two applications.

Thermal management is a crosscutting engineering issue that affects both the power electronics and CIDI programs. The components necessary for high-fuel-economy, low-emission hybrid electric and fuel cell vehicles require that power electronics be smaller and lighter and operate at higher temperatures than those for conventional vehicles. These requirements are being addressed by developing electronic materials (i.e., materials for low-cost dc bus capacitors) that operate at higher temperatures and by improving the capability to dissipate heat generated in electronic devices. The APM Program has been addressing electric drive system heat dissipation issues through the development of advanced carbon foam technology.

Current CIDI engines must strike a delicate balance between high efficiency and low tailpipe emissions. CIDI engine and aftertreatment system development will greatly benefit from the Program's efforts to develop improved engine components and subsystems. The APM Program featured two projects in FY 2003 to develop technology to produce very small (~50 micron) orifices for fuel injectors used in high-pressure common rail systems. The smaller orifices can enable better control of fuel atomization and can increase efficiency and reduce emissions. The Program is also working to reduce emissions through the development of advanced particulate filters and is collaborating with Pacific Northwest National Laboratory in the development of a nonthermal plasma aftertreatment device to reduce NO_x emissions from diesel engines. This is the last year for nonthermal plasma aftertreatment system development within the Program.

Collaboration and Cooperation

As with other programs under FreedomCAR, collaboration and cooperation across organizations is a critical part of the APM Program. Throughout the FreedomCAR Program, scientists at the national laboratories are collaborating with manufacturers to identify and refine the materials characteristics necessary for meeting system performance requirements. Researchers at Lawrence Livermore National Laboratory are working with Ford Motor Company to develop low-cost, rapid-response NO_x sensors that can be used in feedback control loops to monitor and minimize NO_x emissions from diesel engines. There is also cooperation among national laboratories to take advantage of the expertise of each facility.

Oak Ridge and Argonne National Laboratories (ORNL and ANL), for example, are collaborating in the development of higher-strength NdFeB permanent magnets that will enable significant reductions in the size, weight, and cost of electric motors used in hybrid vehicles. In another project, Sandia National Laboratories (SNL) is fabricating smaller, higher-temperature dc bus capacitors; and ORNL is developing techniques to characterize the ~5-micron-thick polymer films developed by SNL and correlate their mechanical properties with their dielectric behavior. These electric drive system projects in turn are regularly reviewed by the EE Technical Team of the U.S. Council for Automotive Research to get feedback on research direction and progress.

In addition to national laboratory and large industry participation, the FY 2003 APM Program included important R&D conducted by a small business. Industrial Ceramic Solutions, LLC (ICS), located in Oak Ridge, Tennessee, is developing a ceramic filter to reduce particulate emissions from diesel engines. As in the collaborative efforts of national laboratories with industry, researchers at ICS are working closely with representatives from DaimlerChrysler, Ford, General Motors, and ORNL to develop a filter that will meet the emissions targets of the program.

Laboratory/contractor-industry collaboration

Laboratory	Industrial Partner			
Argonne National Laboratory	✔	Ability Engineering Technology, Inc.	✔	Daimler-Chrysler Corporation
	✔	Atlas Cylinders, Inc.	✔	Ford Motor Company
	✔	Bronson and Bratton, Inc.	✔	Lucas-Varity
	✔	Cryomagentics, Inc.	✔	Purdue University
	✔	CRUMAX	✔	UGIMAG, Inc.
Oak Ridge National Laboratory	✔	Bronson and Bratton, Inc.	✔	Industrial Ceramic Solutions
	✔	Caterpillar	✔	Motorola
	✔	Conoco Corporation	✔	Murata
	✔	Cryomagnetics, Inc.	✔	Peterbilt
	✔	CRUMAX	✔	Poco Graphite
	✔	Daimler-Chrysler Corporation	✔	UGIMAG, Inc.
	✔	Dow Chemical Company	✔	University of Tennessee
	✔	Ford Motor Company		
	✔	General Motors		
Sandia National Laboratories	✔	AVX	✔	Murata
	✔	Daimler-Chrysler Corporation	✔	Pennsylvania State University
	✔	Ford Motor Company	✔	TAM
	✔	General Motors	✔	Tokay
	✔	Degussa	✔	TPC Ligne Puissance
	✔	Ferro	✔	TPL, Inc.
	✔	Kemet	✔	TRS Ceramics
	✔	Materials Research Associates		

Accomplishments

FY 2003 featured notable accomplishments in both materials program areas. This section highlights some major accomplishments during FY 2003.

Power Electronics

High-power electronic components such as power modules and inverters being developed for hybrid electric and fuel cell vehicles generate significantly more heat than conventional devices. Dissipation of the heat generated by these devices in hybrid electric vehicles requires an additional cooling loop and water-cooled heat sink to prevent overheating and failure of the devices. The increasing power requirements of electronic devices require that more-sophisticated heat sinks be developed to keep the temperature of the electronics below about 120°C. High-

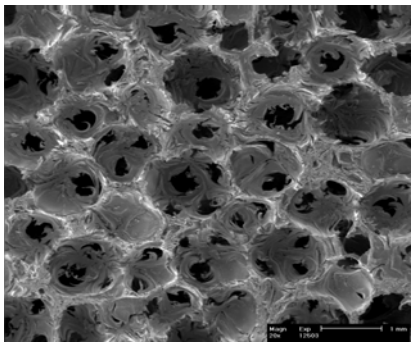

Graphite foam material developed at ORNL

thermal-conductivity, high-surface-area carbon foam is an innovative new material that offers great potential for advanced heat sinks and heat spreaders; however, the high cost of the material is a concern.

An economic model was developed in FY 2003 to help quantify the cost factors in the process for fabricating high-thermal-conductivity carbon foam. More than 50 factors affecting the cost of the foam were identified in this extensive study. The Excel-based model showed that the pitch precursor and graphitization step (temperature, time, furnace size, etc.) had the most dramatic effect on the cost of the foam. The model also provided insight into the sensitivity of expected pitch price to all of the key process and business parameters and therefore served as a tool to guide further development, cost reduction, and commercialization. Research efforts have been redirected to evaluate less costly pitch precursors and simpler graphitization steps.

A collaborative effort between the National Security Agency (NSA) and ORNL has effectively used high-conductivity carbon foam to dramatically increase the cooling capacity of a high-power-density chip system. The lightweight carbon foam has a ligament thermal conductivity comparable to that of diamond wafers but has a surface area that is more than two orders of magnitude greater. When the diamond spreader in the NSA chip assembly was replaced by ORNL's graphite foam, a power density of greater than 110 W/cm^2 was attained without overheating the system. The same technology has been used to develop a low-cost passive heat sink for power modules and inverters.

Advanced Combustion Engine and Emissions R&D

ICS has developed a pleated ceramic fiber filter cartridge to remove hazardous carbon particulates from the exhaust of small diesel engines. This cartridge removes greater than 95% of the diesel soot particles at a fraction of the backpressure of conventional wall-flow filters. (Excess backpressure on a diesel engine is detrimental because it reduces the efficiency of the engine and increases the fuel consumption.) The backpressure of the ICS fiber filter is 1/10 that of a conventional extruded honeycomb filter product. In addition, the thermal mass of the ICS filter is 1/3 that of the honeycomb filter. Thus it requires less auxiliary energy for filter cleaning, again reducing the fuel penalty for the emission control device. These advantages can reduce the fuel consumption penalty from 15% down to 1%. The final advantage is the cost of the product in a high-volume market. The ICS filter is a simple pleated design that is similar to millions of air and liquid filtration devices used around the world. It is manufactured by established processes on high-volume equipment.

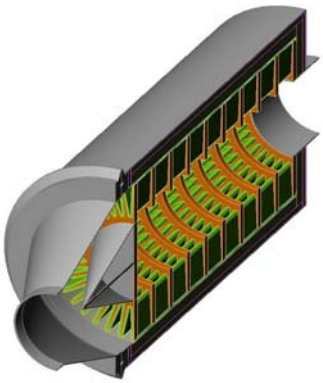

Schematic of ICS particulate trap

ICS is now entering product qualification programs with diesel engine suppliers in the United States and Europe. These suppliers require manufacturing capacity for millions of diesel particulate filter units per year. ICS is in final negotiations with a New York Stock Exchange U.S. filter products company, with international sales, to license the patented technology for volume production. If the qualification tests are successful, it is likely that the low-cost ICS filter will be incorporated into a variety of systems that enable automakers to meet the more-

stringent emissions requirements in the United States in 2007 and in Japan and Europe in 2008.

Another method for reducing particulate emissions from diesel engines is to improve fuel atomization. This can be accomplished in a number of ways: by increasing the fuel injection pressure, by sophisticated control of the injection timing, and/or by reducing the diameter of the orifices through which fuel is injected into the cylinder. Increasing the injection pressure is problematic because of safety concerns and the increased risk of cracking the injectors. Control systems—particularly those requiring specialized sensors for monitoring the combustion process—can add to the complexity and expense of the engine. Research has shown that the use of injectors with orifice diameters of around 50 µm should result in significant reductions in particulate emissions; however, no processes are available for fabricating such fuel injectors.

Work conducted at ANL in FY 2003 demonstrated the feasibility of using electroless nickel plating to reduce the injector orifice diameter of standard injectors from 200 µm to about 50 µm by depositing thick, uniform layers of nickel plate along the interior surfaces of the injector orifices. Electroless nickel plating is a mature technology, but it has not been used in this application before. It is highly scalable and appears to be an economical technique for fabricating small-orifice injector nozzles. In addition to achieving major reductions in orifice diameter, ANL research has shown that electroless nickel deposition reduces the surface roughness of the orifice interior. Changes in the plating bath chemistry have also been shown to vary the hardness of the nickel plate, suggesting the possibility of tailoring the hardness so as to reduce cavitation and erosion. In addition, bench tests indicate that electroless nickel coatings are about 50% less susceptible to deposit formation than the base metal of the injector.

Typical diesel fuel injector nozzles

Future Direction

The APM Program will continue to work closely with FreedomCAR partners and industry to understand propulsion materials–related requirements. Building upon the recent advances in materials technologies, many of this year's projects will be moved out of the laboratory and over to industry for testing. Strategic partnerships will be established in 2003 with exhaust system, engine, or vehicle manufacturers to move the particulate filter system from vehicle testing toward commercialization. The scale-up and commercialization of carbon foam at POCO Graphite for thermal management applications will continue, with the focus on cost reduction. Other projects will continue to refine manufacturing requirements and necessary characteristics to meet the challenges of the FreedomCAR program.

As advanced automotive technology developments uncover new challenges, the APM Program will continue to provide breakthrough technology solutions through collaboration with industry, FreedomCAR partners, national laboratories, and small businesses.

Project Abstracts

The remainder of this report communicates the progress achieved during FY 2003 under the APM Program. It consists of ten abstracts of national laboratory projects—six that address power electronics and four that address combustion and emission technologies. The abstracts provide an overview of the critical work being conducted to improve these systems, reduce overall cost, and maintain component performance. In addition, these abstracts provide insight into the challenges and opportunities associated with advanced materials for high-efficiency automobiles.

Rogelio Sullivan

Team Leader, Materials Technologies
Office of FreedomCAR and Vehicle Technologies
Energy Efficiency and Renewable Energy

2. POWER ELECTRONICS

A. Low-Cost, High-Energy-Product Permanent Magnets

Y. S. Cha and John R. Hull
Energy Technology Division, Bldg. 335
Argonne National Laboratory, Argonne, IL 60439
(630) 252-5899; fax: (630) 252-5568; e-mail: yscha@anl.gov

E. Andrew Payzant
Oak Ridge National Laboratory
P.O. Box 2008, MS 6064
Oak Ridge, TN 37831-6064
(865) 574-6538; fax: (865) 574-3940; e-mail: payzanta@ornl.gov

DOE Technology Development Manager: Susan Rogers
(202) 586-3976; fax: (202) 586-9811; e-mail: susan.rogers@ee.doe.gov
ORNL Technical Advisor: David Stinton
(865) 574-4556; fax: (865) 241-0411; e-mail: stintondp@ornl.gov

---

Contractor: Argonne National Laboratory, Argonne, Illinois
Prime Contract No.: W-31-109-Eng-38

Objective

- Develop a low-cost process to fabricate anisotropic NdFeB permanent magnets (PMs) with an increase of up to 25% in energy product (a measure of the torque that a motor can produce for a given magnet mass).

Approach

- Use high fields of superconducting solenoids to improve magnetic grain alignment while pressing compacts for sintering, thus producing higher-performance magnets.
- Develop a batch-mode press that enables alignment of the magnetic domains of NdFeB powders in the higher-strength magnetic fields created by a superconducting solenoid.
- Characterize, compare, and correlate engineering and microscopic magnetic properties of magnets processed under varying conditions, including some in current production.
- Use a reciprocating feed to automate the insertion of loose and compacted magnet powder into, and its removal from, the steady magnetic field of a superconducting solenoid.

Accomplishments

- Achieved energy products within 10% of the theoretical maximum by optimizing batch-mode alignment/pressing of cylindrical axial-die-pressed PMs in a 9-Tesla (T) superconducting solenoid. The magnetic properties are comparable to those of the more expensive magnets made by the transverse-die pressing technique.

- Achieved energy product improvements of 15% for thin near-final-shape magnets, production of which is the current cost-saving thrust in the PM industry. Additional PMs made with relatively small length-to-diameter ratios (L/D <0.5) support the previous findings.
- Completed preliminary conceptual design of a vacuum die-filling and powder-pressing system to alleviate cracking that was observed in fabricating compacts with low L/D ratios (<0.25). The vacuum system will also speed up the powder-filling and pressing process, necessary for industrial acceptance of this new technology.
- Carried out an electromagnetic modeling study of grain alignment in powder compacts. Analyses were carried out by assuming that all the magnetic particles are either initially oriented in the direction of the alignment field or initially randomly oriented. The results of both analyses show that the distortion of the alignment field (caused by the self-field of the compact) is inversely proportional to the magnitude of the alignment field. These results will help to provide scale-up design rules to industry.

Future Direction

- Complete the design and fabrication of the vacuum powder-filling and compact-pressing system and of the pressurized compact ejection system. Demonstrate that compacts can be made at rates acceptable to industry.
- Conduct an economic study comparing the estimated cost of PM manufacturing in continuous-mode operation using the superconducting magnet, with the cost of a conventional system currently used by industry.
- Continue to collaborate with Magnequench UG on PM fabrication and property measurements, with Oak Ridge National Laboratory (ORNL) on microstructure characterization of the finished PM samples, and with Ames Laboratory on processing the NdFeB powder for bonded PMs.

Introduction

The strength of sintered NdFeB magnets greatly depends on the method by which the compact is magnetically aligned and pressed. Large blocks can be made by cold-isostatic pressing that are within 5% of their theoretical maximum, but these must be sliced, diced, and ground to final shape, making the magnets very expensive. Magnets that are axial-die-pressed and sintered to near-final shape are the least expensive to make, but they have magnetic properties farthest from their theoretical maximums. The current industry goal is to fabricate higher-energy-product magnets by near-net-shape processing to avoid expensive machining operations. The major objectives of this project are to increase the energy product of the sintered PMs by 10 to 15% (to within ~10% of the theoretical maximum) and to develop low-cost methods of production for high-energy-product, near-final-shape PMs. The higher-performance magnets will replace ones made by traditional powder metallurgy processing and enable significant size and weight reductions in traction motors for hybrid vehicles.

Approach

Our approach is to align the NdFeB powder in a superconducting magnet, which can generate magnetic fields much higher than those generated by the electromagnets presently used in industry. Alignment of the powder in these higher magnetic fields improves the properties of the PMs. To develop a low-cost mass-production method for high-energy-product PMs, we plan to design, fabricate, and demonstrate the reciprocating axial-die-press system for automation.

Previously, a 9-T superconducting solenoid was procured and made operational. Production-grade magnet powder was obtained from Magnequench UG. The 3- to 5-micron single-crystal grains of powder were aligned and compacted at Argonne National Laboratory (ANL). Then the anisotropic compacts, with their grains mechanically locked in place, were returned to Magnequench UG for sintering, annealing, machining, and measuring of engineering magnetic properties. Finally, selected PMs were sent to ORNL for measurement of microscopic properties and texture (the alignment of the crystals' easy magnetic axes).

Previously, we had demonstrated that significant improvement of energy product (10–15%) can be achieved by using higher alignment fields (>2 T).[1] Industry considers an improvement in energy product of as little as 3–5% compared with current PMs to be significant. The progress achieved so far is based on a batch process at ANL. Major issues remaining for acceptance of the technology by industry are (1) to demonstrate that PMs can be made at a much faster rate than in the batch process and (2) to demonstrate that near-final-shape PMs can be processed, resulting in greater cost reduction.

Results

In FY 2003, we continued the previous study with emphasis on a smaller L/D ratio (<0.25) where improvement in energy product is expected to be greater. The most effective use of the high alignment fields that can be provided by superconducting solenoids is in making near-final-shape magnets. Their finite and usually short length in the direction of magnetization makes alignment of the powder grains especially difficult. When subjected to a uniform alignment field, the powder in the die cavity develops a highly nonuniform self-field. Because grains align along the total field lines, unidirectional alignment can be achieved only by increasing the strength of the applied alignment field until the effects of the self-field become negligible. Because the self-field distortion becomes greater for shorter magnets, there will always exist short magnets that conventional 2-T electromagnets cannot adequately align.

A 1.125-in. die and punch system was used in the present study in order to achieve an L/D ratio smaller than 0.25. A large number of powdered compacts were processed under various conditions. However, all the samples were observed to have hairline cracks after ejection from the die and eventually broke into pieces. Figure 1 shows one of the cracked samples.

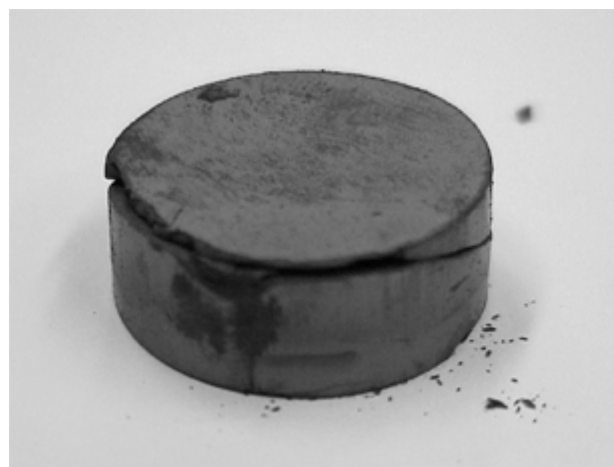

Figure 1. Photograph of a cracked compact after ejection from the die.

A number of factors could have caused the powered compacts to crack (some were suggested by our industrial partner, Magnequench UG). They include

- Maximum compact pressure and duration
- Rate of pressure loading and unloading (trapped air)
- Powder fill density
- Lubricant (type and amount)
- Magnetic field for alignment
- Die/punch geometry (e.g., clearance, punch diameter, taper angle of die)
- Oxygen content

- Powder homogeneity and filling procedure
- Compact ejection pressure

We have investigated all these factors and have concluded that the most likely causes for compact cracking are either air trapped during powder compaction and/or radial stress during compact ejection from the die. The production-grade magnet powder, received from Magnequench UG, is porous and contained a lot of air. If sufficient time and clearance are not provided during powder compaction, air will be trapped in the compact. The trapped air can subsequently cause the compact to crack when the pressure is released. This is a well-known problem for this type of process. The other likely cause for compact cracking is the radial stress during compact ejection from the die. Figure 2 shows the stresses on the compact during pressing and during compact ejection for the current system. During compact ejection, the axial stress is released while the radial stress is still very large; this could cause the compact to crack.

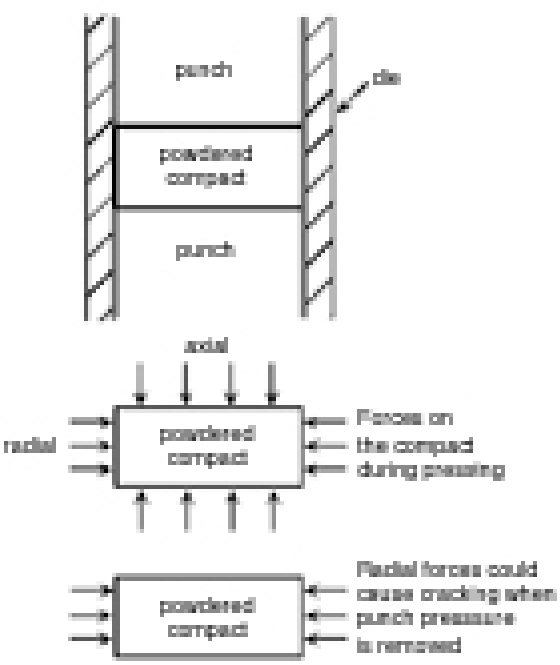

Figure 2. Schematic diagram showing probable cause of cracking during compact ejection from the die.

The industrial practice is to eject the compact under axial pressure. In order to eject the compact under pressure, the current set-up must be upgraded.

To address the issues of trapped air and compact ejection under pressure, we came up with an innovative method of filling the die and pressing the compact under vacuum. Using the vacuum system will reduce the trapped air in the powder significantly, which (1) may alleviate the cracking problem, (2) will increase the powder-pressing speed, and (3) will speed up the powder-filling process. The last two improvements are also a necessary step toward demonstration of a process that can manufacture PMs at a much faster rate than the batch mode. By using the vacuum-compatible die, we also came up with a preliminary conceptual design for a system that can eject the compact under pressure, which may alleviate the cracking problem described previously.

To understand the effect of the self-field of the magnet powder on the distortion of the alignment field, we carried out an electromagnetic study of grain alignment in powder compacts using the computer code Opera developed by Vector Fields, Inc. Previously, we conducted the analysis by assuming that all the magnetic particles are initially oriented in the direction of the alignment field. The results provided a lower bound on the distortion of the field lines. In the present analysis, we assume more realistically that the magnetic particles are initially randomly oriented. Figures 3 and 4 show the calculated field lines of one-quarter of a PM for alignment fields of 1 and 8 T, respectively. These calculations were carried out using the same powder density (3.5 g/m^3) and the same L/D ratio (0.643). The field lines will all be parallel to the z-axis if there is no distortion. It is clear that distortion of the alignment field is substantial when the alignment field is 1 T (Figure 3). The distortion decreases with increasing alignment field. At an alignment field of 8 T, the distortion becomes very small (Figure 4).

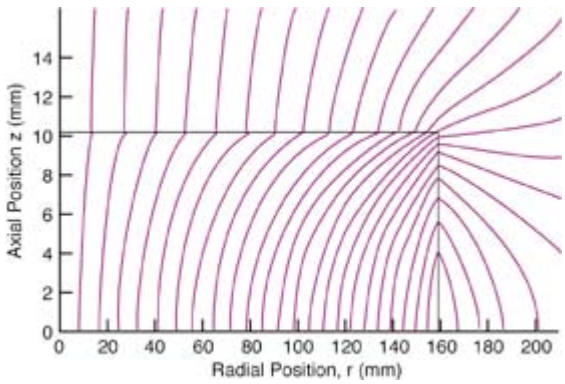

Figure 3. Field lines (one-quarter) for compact partially pressed to mechanical lockup. Alignment field H =1 T. Parameters: ρ_1 = 3.5 g/m^3, L/D = 0.643, B_0 = 0.65 T.

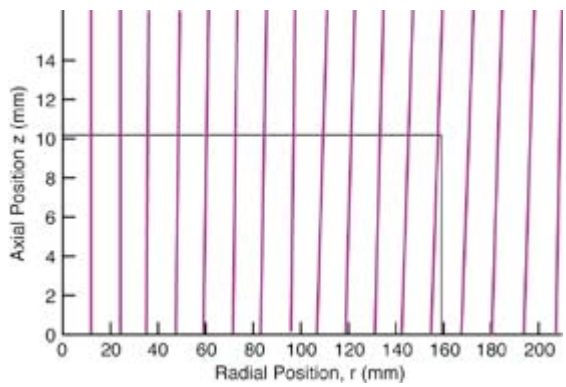

Figure 4. Field lines (one-quarter) for compact partially pressed to mechanical lockup. Alignment field H = 8 T. Parameters: ρ_1 = 3.5 g/m^3, L/D = 0.643, B_0 = 0.65 T.

Figure 5 shows the comparison of the field line distortion between the previous analysis (assuming magnetic particles are initially oriented in the direction of the alignment field) and the current analysis (assuming magnetic particles are initially randomly oriented). B_r and B_z are defined as the radial and the axial components of the magnetic flux density B, respectively. The vertical axis represents the volume average of the ratio B_r/B_z, which is a good measure of the overall distortion of the field lines. As expected, Figure 5 shows that the distortion of the field lines is greater if the magnetic particles are initially randomly oriented,

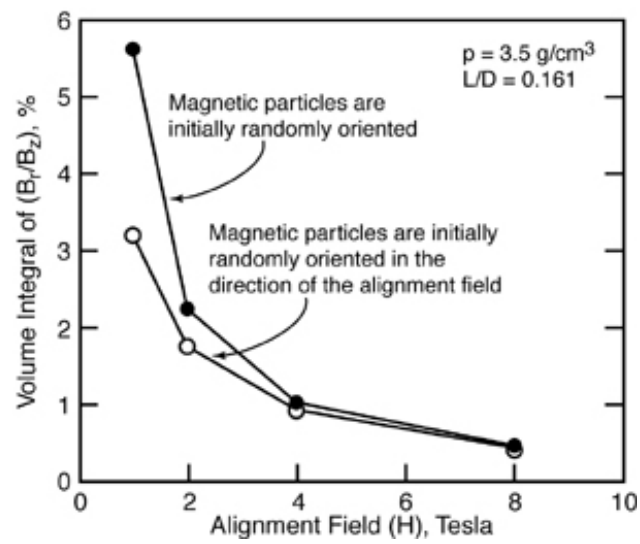

Figure 5. Comparison of field line distortion between previous and present analyses.

compared with the case where the magnetic particles are initially oriented in the direction of the alignment field. Both analyses show that the distortion of the field lines decreases with increasing alignment field.

Conclusions

Previously, we demonstrated that significant improvement of energy product (10–15%) can be achieved by using higher alignment fields (>2 T). Industry considers an improvement of 3–5% in the energy product of current PMs to be significant. Major issues remaining for acceptance of the technology by industry are (1) to demonstrate that PMs can be made at a much faster rate than in the batch process, and (2) to demonstrate that near-final-shape PMs can be processed, resulting in greater cost reduction. In FY 2003, we continued to fabricate powdered compacts with an even smaller L/D ratio (<0.25) by using a larger (1.125–in.) die and punch set. However, all the samples were observed to have cracks after ejection from the die. With the help of industrial partner Magnequench UG, we identified two factors that probably caused the compacts to fail: trapped air in the

powdered compact during pressing and the radial stress during ejection of the compact from the die.

To alleviate the trapped air problem, we decided to use a vacuum-compatible die. We have completed a preliminary conceptual design of a vacuum die/punch set. The system also allows the present system to be modified so that the compact can be ejected under pressure, which also may alleviate the cracking problem. We have completed a preliminary conceptual design for upgrading the existing system for just this purpose.

To help us understand and quantify the distortion of alignment field due to the self-field of the magnet powder, we continued the electromagnetic study of grain alignment in powder compacts using the computer code Opera. Previously, we assumed that all the magnetic particles are initially oriented in the direction of the alignment field. In the present analysis, we assume more realistically that the magnetic particles are initially randomly oriented. As expected, the results show that the distortion of the field lines is greater if the magnetic particles are initially randomly oriented. Both analyses show that the distortion of the alignment field lines decreases with increasing alignment field.

In FY 2004, we plan to complete the design, fabricate the vacuum die/punch set, and demonstrate that PMs can be manufactured at a much faster rate than with the batch process. We will also perform an economic study comparing the estimated cost of the present superconducting system with that of the conventional system used by industry. Our long-term and final goal is to demonstrate the feasibility of competitive factory operation by designing, fabricating, and operating a reciprocating press in continuous-mode operation.

References

1. *2002 Annual Progress Report, Automotive Propulsion Materials*, U. S. Department of Energy, Office of Energy Efficiency and Renewable Energy, Office of FreedomCar and Vehicle Technologies, Washington, D.C.

FY 2003 Publications/Presentations

T. M. Mulcahy, J. R. Hull, E. Rozendaal, J. H. Wise, and L. R. Turner, "Improving Sintered NdFeB Permanent Magnets by Powder Compaction in a 9-T Superconducting Solenoid," presented at the 47th Annual Conference on Magnetism and Magnetic Materials, Tampa, Florida, November 11–15, 2002 (to be included in the proceedings).

T. M. Mulcahy, J. R. Hull, E. Rozendaal, J. H. Wise, and L. R. Turner, "Improving Sintered NdFeB Permanent Magnets by Powder Compaction in a 9-T Superconducting Solenoid," *J. App. Phys.* **93**(10), pt. 3, 8680–82 (2003).

Y. S. Cha and J. R. Hull, "Low-cost High-energy-product Permanent Magnets," presented at the Capacitor and Magnetic Materials, Power Electronics/Electric Machinery Program Review, U.S. Council on Automotive Research, Southfield, Michigan, May 13, 2003 (to be included in the proceedings).

B. Development of Improved Powder for Bonded Permanent Magnets

Iver E. Anderson, R. William McCallum, and Matthew J. Kramer
Metallurgy and Ceramics Program
Ames Laboratory, Iowa State University
Ames, IA 50011
(515) 294-9791; fax: (515) 294-8727; e-mail: andersoni@ameslab.gov

DOE Technology Development Manager: Susan Rogers
(202) 586-8997; fax: (202) 586-1600; e-mail: susan.rogers@ee.doe.gov

---

Contractor: Ames Laboratory, Iowa State University, Ames, Iowa
Prime Contract No.: W-7405-Eng-82

Objectives

- Increase the maximum operating temperature of permanent magnet (PM) electric drive motors from 120 to 200°C while maintaining sufficient motor operating characteristics.
- Reduce the cost of isotropic PM material in electric drive motors through the use of bonded isotropic magnets and injection molding technologies for high-volume net-shape manufacturing.

Approach

- Develop innovative PM alloy design and processing technology for production of improved PM alloy powders for bonded isotropic magnets with a tolerance for high temperatures.
- Investigate PM alloy design improvements through melt-spinning methods, with the specific goal of developing an improved spherical magnet alloy powder through gas atomization processing.
- Develop an enhanced gas atomization process, along with a gas-phase powder surface reaction capability, for production and environmental protection of powder for isotropic bonded magnets.
- Conduct experimental isotropic PM molding trials on as-atomized and annealed magnet powders to characterize isotropic bonded magnet properties and microstructures in collaboration with Magnequench International (MQI) and Oak Ridge National Laboratory (ORNL).

Accomplishments

- Filed a U.S. patent application for a new mixed rare earth (MRE)–Fe-B family of 2-14-1 compounds with demonstrated high-temperature magnetic stability, better than that of commercial isotropic materials, for PM traction motors based on bonded magnets.
- Identified a promising path forward for MRE–Fe-B alloy design to increase the remanence and energy product for isotropic PMs while maintaining superior temperature coefficient values.
- Observed that post-atomization annealing may not be needed to improve the magnetic properties of spherical MRE–Fe-B powders, potentially a significant processing simplification that also can facilitate the fluoride coating process.

- Performed direct comparative testing of bonded magnet samples molded from experimental gas-atomized fine spherical powders and commercial atomized powders, aided by interaction with MQI, a major commercial supplier.

Future Direction

- Pursue an alloy design strategy for MRE–Fe-B to increase the remanence and energy product for isotropic PM material, while maintaining superior temperature coefficient values to 200˚C, using a melt-spinning approach. Use commercial isotropic particulate properties and motor designer input as benchmarks.
- Test enhanced MRE–Fe-B alloy designs in gas-atomized spherical powders to verify magnetic property improvements in as-solidified and annealed states. Use microstructural analysis to investigate the differences between rapidly solidified ribbons and powders with the goal of simplified production of optimum powder.
- Refine the fluidized bed fluorination process for gas-atomized MRE–Fe-B powder to optimize the coating barrier properties for protection of PM powders during the magnet molding process and bonded magnet use.
- Generate bonded magnet samples with increased (> 60%) loading for comparative magnetic testing from a polyphenyl sulfide binder blended with experimental or commercial PM powders. Develop (in collaboration with an industrial partner) a molding process for producing a prototypical motor part with a filled magnet cavity to investigate the effects on the molding process of powder/polymer blend characteristics, attempting to achieve maximum magnet loading within acceptable molding parameters.

Introduction

To meet the cost and performance objectives of advanced electric drive motors for automotive applications, it is essential to improve the alloy design and processing of PM powders. This work is critical to enable the widespread introduction of electric drive automobiles, generally referred to as hybrids or fuel cell vehicles, a key technology goal of the President of the United States and of DOE. Two primary objectives to be pursued for PM materials are (1) to increase the useful operating temperature for magnets to 200˚C and (2) to reduce the finished magnet cost to about 25% of its current level. Currently, high-performance anisotropic sintered magnet material can operate with high torque in an electric motor at temperatures ranging up to about 120˚C, and the finished cost of anisotropic sintered magnetic material is approximately $90/kg. Difficult motor assembly procedures and the need for corrosion protection (by surface coatings) also add to the cost for PM motors made from sintered anisotropic PMs. As an alternative PM material form, polymer-bonded isotropic particulate magnets offer the benefit of greatly simplified manufacturing and improved (polymer encapsulation) corrosion protection. Compared with anisotropic sintered magnets, they provide a more moderate level of stored magnetic energy (25–50%), which is still compatible with advanced PM motor designs. However, to exploit the potential of bonded isotropic PM materials for such motors, it is necessary to develop a particulate magnet material with high-temperature properties that can be loaded to a high volume fraction in an advanced polymer binder. Improving materials and processing to enable increased operating temperatures and simplified production of net-shape bonded isotropic magnets by gas atomization and injection molding will be a significant advance toward mass production of advanced electric drive motors at reduced cost.

Approach

Innovative PM alloy design and processing technology will be developed for production of improved PM alloy powders based on the $Nd_2Fe_{14}B$, or "2-14-1" phase for bonded isotropic PM magnets with a tolerance for high temperatures. Melt spinning will be used to select alloy modifications that boost coercivity, remanence, and energy product at elevated temperatures (up to 200°C) and improve alloy quenchability for optimum yield from a gas atomization process.

This effort builds on an alloy concept patented by Ames Laboratory for improved quenchability of the neodymium (Nd)-based 2-14-1 phase using, for example, TiC. A high-pressure gas atomization process was modified for enhanced yields of spherical, rapidly solidified powder of improved PM alloys. This atomization work uses the patented Ames Laboratory technologies for bonded magnets from passivated fine spherical powders. A secondary gas-phase reaction coating process is being developed to increase environmental protection of the fine magnet alloy powder without degrading the magnetic properties or molding rheology. This work builds on recent studies of fluidized bed fluorination of similar rare earth (RE) alloy powders. A model polymer, polyphenyl sulfide (PPS), was selected and is being used to test injection molding characteristics and magnetic properties of high-temperature bonded isotropic magnets.

The magnetic properties of bonded isotropic powder samples will be determined as a function of loading fraction, powder size, annealing schedule, coating treatment, and temperature, up to a maximum of 200˚C, in collaboration with industrial partner MQI of Raleigh-Durham, North Carolina. Some of the atomized powder and bonded isotropic magnets also will be provided to ORNL for additional microstructural and magnetic characterization. To improve further the potential for successful technology transfer, industrial interactions have been emphasized at Ames Laboratory. These include work with MQI on alloy design and rapid solidification processing through a DOE cooperative research and development agreement (CRADA) on advanced sensors and control of the melt-spinning process, and other CRADA projects and research collaborations with U.S. Council on Automotive Research partners.

Results

In FY 2003, the Iowa State University Research Foundation filed a U.S. patent application on November 18, 2002, for a "Permanent Magnet Alloy with Improved High Temperature Performance." Even non-optimized MRE–Fe-B PMs based on this invention have demonstrated exceptional resistance to high-temperature demagnetization, with useable magnetic properties up to 250˚C, beyond the target temperature range of this project. The scientific basis of the work reaches back to fundamental characterization of 2-14-1 compounds made from the complete range of possible RE elements, along with Fe and B additions. It was recognized that a mixture (probably substitutional and random) of alternative RE elements in a 2-14-1 phase may have an average of the magnetic properties of the well-known $Nd_2Fe_{14}B$ phase, as shown in Figure 1. Such MRE–Fe-B compounds appear to offer some new alloy design territory that can be exploited for raising the useful temperature range for high magnetic performance in this type of PM phase. The prototype of this new family of MRE–Fe-B magnet alloys is composed of an equi-atomic mixture of Y and Dy in the 2-14-1 stoichiometric compound of $YDyFe_{14}B$. A thorough search of the open literature verified that this type of compound is novel and thus suitable for patent filing.

Melt spinning was used to generate a range of rapidly solidified ribbon samples with compositions within the range of the novel MRE–Fe-B PM alloy family. Wheel

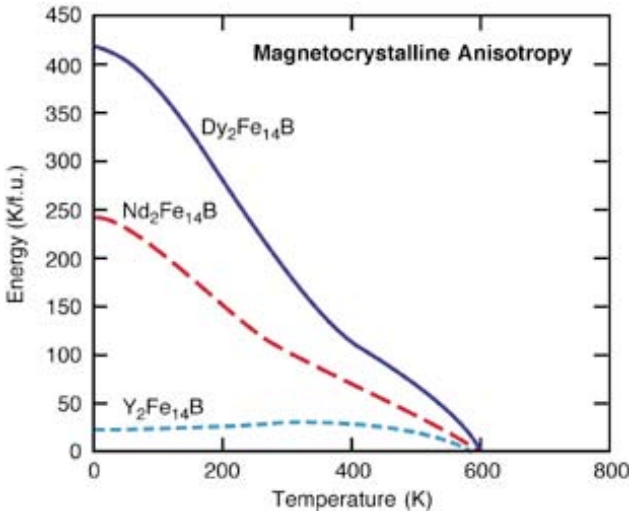

Figure 1. Illustration of the intermediate temperature dependence of the anisotropy of Nd-based 2-14-1 phase, showing the potential for high-temperature magnet alloy design with mixed REs, e.g., Y and Dy.

speeds of 10, 16, and 22 m/s were used to simulate the range of gas atomization quench rates from argon to helium gas. Annealing temperatures were tested from 650 to 850˚C to seek beneficial solidification and annealing conditions to use for subsequent spherical powder processing. X-ray diffraction (XRD) measurements indicated that the as-solidified ribbons contained a phase mixture of MRE_2Fe_{17} phase, some 2-14-1 phase, and a minor amorphous phase fraction, without any reflections from bcc-Fe. Upon annealing, XRD data show that the magnetic microstructure transformed into essentially single-phase 2-14-1. The magnetic hysteresis loop of an annealed ribbon sample of the $YDyFe_{14}B$ compound is illustrated in Figure 2, which also shows the reduced effect of elevated temperature on the magnetic properties.

To explore the trends suggested in Figure 1, some ribbon samples were made with a heavier balance of Y, compared with Dy. The expectation was a lower coercivity and energy product but a further-decreased temperature dependence of the magnetic properties compared with the equi-atomic

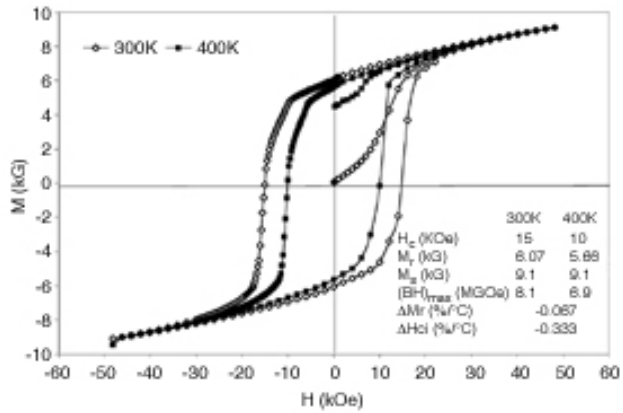

Figure 2. SQUID magnetometer measurements of a melt-spun (@22 m/s) ribbon sample of $YDyFe_{14}B$ that was annealed at 700˚C for 15 min and measured at 27 and 127˚C, where a 15% loss of energy product was observed for a 100˚C temperature rise.

mixture of Y and Dy. As Figure 3 shows, the energy product was only slightly reduced and coercivity was slightly increased. Also, the temperature effect was slightly higher than expected. Apparently, this MRE compound has an increased range of tolerance for alloy adjustments, which needs further testing.

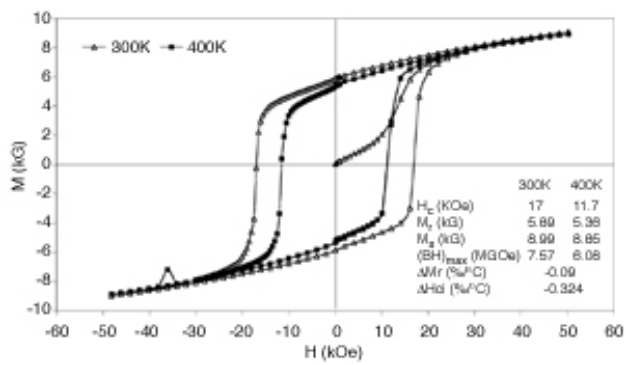

Figure 3. SQUID magnetometer measurements of a melt-spun ribbon sample of $Y_{1.35}Dy_{0.95}Fe_{14}B$ (Y-rich) that was annealed at 650˚C for 15 min and measured at 27 and 127˚C, where a 20% loss of energy product was observed for a temperature rise of 100˚C.

In recent work, melt spinning was used to explore the effect on magnetic properties of a range of Nd additions, known to promote 2-14-1 remanence, using an alloy formulation of $[Nd_x(YDy)_{1/2(1-x)}]_{2.2}Fe_{14}B$. The intent was to seek an understanding of the magnetic property dependence of this extended MRE–Fe-B formulation, with the goal of improved remanence and energy product without adverse effects on the desirable temperature coefficients for coercivity and remanence. As expected from relative magnetic moment data, a rising trend of the ambient temperature energy product was observed with Nd additions to a level at $\times = 0.8$ of about 11 MGOe, almost double the initial value of about 6 MGOe (Figure 4). The coercivity exhibited a falling trend over the same range of Nd content, but the lowest level of about 14 kOe is still appreciable for many magnet applications. The temperature coefficients displayed a more nonlinear behavior, but the ability to adjust these properties was also apparent. More study of similar alloy series will permit rapid identification of promising compositions for continued powder processing experiments using gas atomization.

Following trials to determine processing corrections to the nominal composition, gas-atomized powder of the prototype $YDyFe_{14}B$ composition of our novel magnet alloy was produced under high quenching conditions (helium atomization gas) and tested at ambient and elevated temperature as a function of powder size and annealing treatment. XRD measurements of the as-solidified powder indicated that 2-14-1 compound was essentially the only product phase without any detectable amorphous phase, even in the finest powder size fraction.

In full agreement with the XRD results, it was discovered that the as-atomized $YDyFe_{14}B$ powder did not need annealing to enhance magnetic properties, contrary to the behavior of melt-spun ribbon of the same composition, as discussed earlier. As Figure 5 illustrates, the only result of annealing appeared to be a slight reduction of coercivity that is typically associated with coarsening of the 2-14-1 grain size. In other words, the atomized droplet solidification process appears to produce directly a desirable magnetic microstructure, without the need for an additional high-vacuum

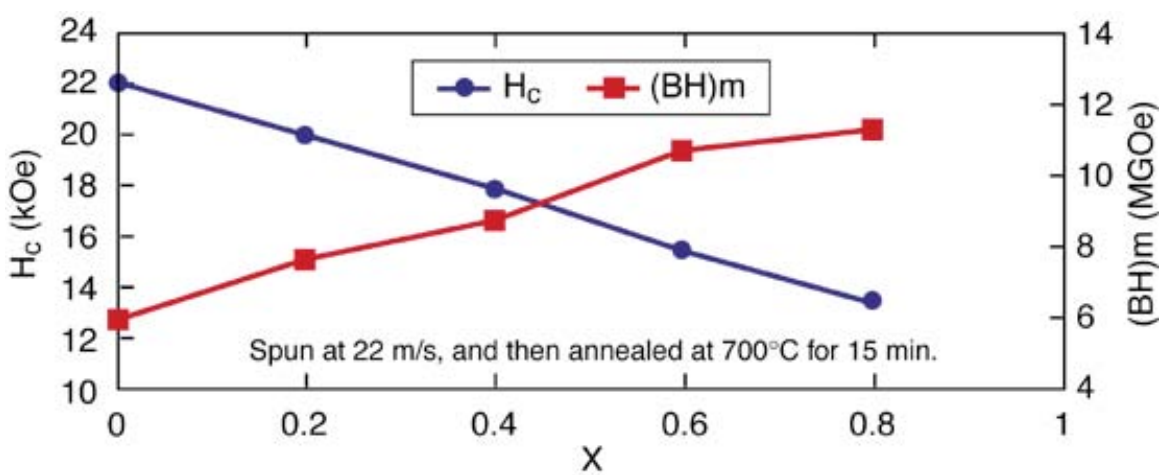

Figure 4. Summary of the effect of Nd additions to an $[Nd_x(YDy)_{1/2(1-x)}]_{2.2}Fe_{14}B$ alloy, using melt-spun ribbon samples, on (a) ambient temperature (27°C), coercivity, and energy product and (b) the temperature coefficients for coercivity and remanence, measured between 27 and 127°C.

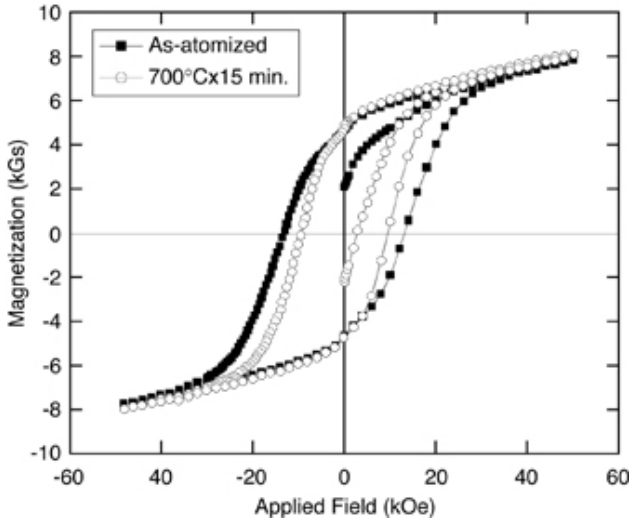

Figure 5. SQUID magnetometer results that show the effect of annealing on as-atomized $YDyFe_{14}B$ powder that had been sieved at 20 µm to exclude larger particles.

heat-treatment procedure with a highly controlled dwell time. The implications of this observation, if verified for other alloy compositions in the MRE–Fe-B alloy family, can be significant for industrial powder processing simplification and thus for cost reduction of the resulting bonded magnets.

In other characterization results for the helium-atomized $YDyFe_{14}B$ powder, unannealed powder was divided into a wide range of size fractions for magnetometer testing. As shown in Figure 6, while the finest powder had a high coercivity of 13 kOe, even some of the larger particle size classes exhibited a coercivity greater than 10 kOe. In fact, size distribution analysis of the full powder yield from this atomization trial indicates that 90% (by mass) of the as-atomized powder yield has a diameter of <45µm and, as Figure 6 shows, a coercivity above 9.5 kOe. Thus only a simple screen cut, instead of pneumatic size classification, would be needed, presumably, to prepare this powder for coating and bonding. This type of observation, if verified for more optimized alloys, would have additional beneficial effects on bonded magnet cost reduction.

One key indication of a promising PM alloy for high-temperature service is a reduction in the downward slope with increased temperature of coercivity and remanence, expressed as temperature coefficients ΔHci and ΔMr, respectively. All of the commercial materials listed in Table 1 are offered for use in bonded magnets and can serve as a useful benchmark. Numerous experimental melt-spun and atomized

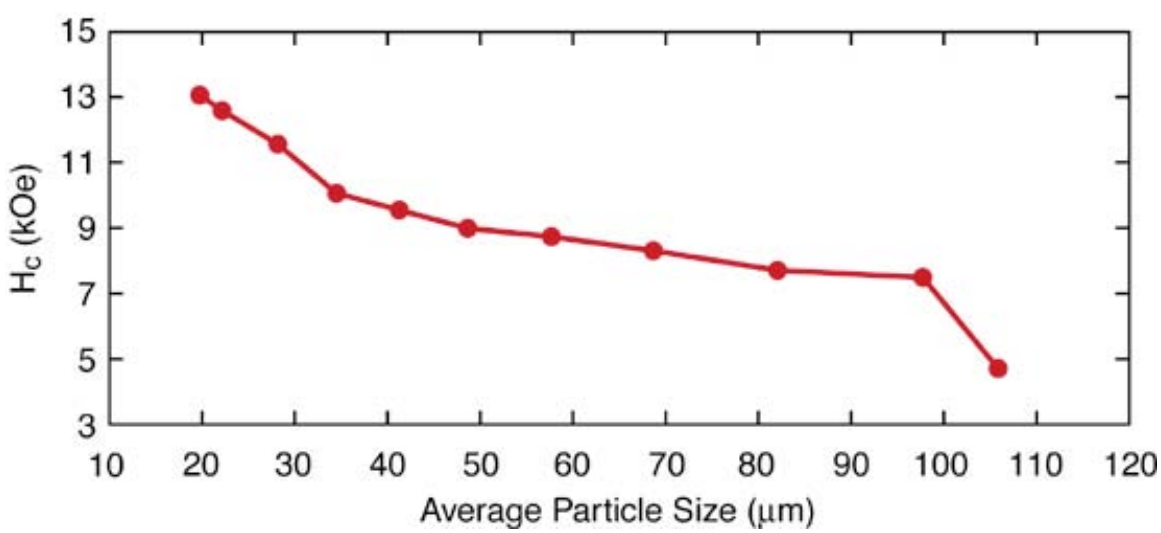

Figure 6. Effect of particle size on the coercivity of as-atomized $YDyFe_{14}B$ powder.

Table 1. Summary of magnetic properties and temperature coefficients for representative commercial (MQ prefix, from MQI) and experimental alloys (as listed) in both melt spun ribbon particulate form and atomized spherical powder form (underlined)

Material	M_r(kG)	H_{ci}(kOe)	$(BH)_{max}$	ΔM_r (%/°C)	ΔH_{ci} (%/°C)
MQP-S-9-8	7.2	9.5	10.0	–0.11[a]	–0.4[a]
MQP-S-11-9	7.6	9.4	11.5	–0.13[a]	–0.4[a]
MQP-O	8.2	14	14.0	–0.13[a]	–0.4[a]
MQP-B	8.95	10	15.8	–0.11[a]	–0.4[a]
$YDyFe_{14}B$ (X5-132B)	6.1	15	8.1	–0.07[b]	–0.33[b]
$YDyFe_{13}CoB$ (X5-201A)	6.3	12.3	7.5	–0.03[b]	–0.33[b]
$Y_{1.35}Dy_{0.95}Fe_{14.6}B$ (MWF43A)	5.89	17	7.6	–0.09[b]	–0.32[b]
$Nd_2Fe_{14}B$-TiC (BT-4-138)	7.2	10.8	6.8	–0.16[b]	–0.38[b]
$YDyFe_{14}B$ (BT-4-204)	4.7	13	4.4	–0.085[b]	–0.33[b]

[a]Measured from 22 to 100°C.

[b]Measured from 27 to 127°C

samples with a variety of compositions (examples provided in Table 1) were subject to ambient and elevated temperature SQUID magnetometer measurements, which determined a desirable reduction in ΔHci values (from 27 to 127°C), compared with those values for commercial melt-spun and atomized particulate (from 22 to 100°C). Moreover, the ΔMr values for all experimental MRE-based alloys were reduced considerably, compared with the commercial materials. The exception is the Nd-based atomized powder (with a composition similar to that of the commercial materials) that had a comparable ΔMr and most other magnetic properties. Generally, the MRE experimental alloys exhibited increased coercivity, but improvements in remanence and energy product are needed to exceed the commercial-standard materials. Systematic modifications of the experimental alloys are being pursued to gain the understanding needed to enhance the full range of magnetic properties to enable superior high-temperature bonded magnets.

An additional requirement for high-temperature bonded magnets is the ability to resist oxidation and corrosion in the environment of a polymer molding process and during service in a "semi-permeable" polymer matrix. This is especially important to enable bonding of fine atomized powders with a high surface-to-volume ratio without sacrificing active magnetic volume. The fluorination coating process under development is based on low-temperature (about 200˚C) reaction of magnet alloy powder in a fluidized bed with NF_3 gas. This coating has promise for a wide range of environmental conditions, but air oxidation appeared to represent a sufficient screening test for the coated powders. Thermo-gravimetric analysis results on annealed and fluoride-coated Nd-based gas-atomized powders demonstrated a 50°C increase in air oxidation stability for powders with diameters of < 25µm. To ensure that only a minor fraction of the spherical powder volume was affected by the coating reaction, the powder surfaces were analyzed with scanning electron microscopy, as shown in Figure 7, and Auger electron spectroscopy. These results revealed no surface disruption or rumpling and a fluoride penetration depth of only 15 nm, well within the range of desirable surface film coverage. Initial fluorination processing experiments on unannealed $YDyFe_{14}B$ powders indicated a reduced reaction temperature, compared with the Nd-based powders; and the resulting coating exhibits similar increases in air oxidation resistance, compared with uncoated powders. Tests for fluoride coating thickness (Auger) are in progress. When final alloy design permits full development of the fluoride coating process, this capability is

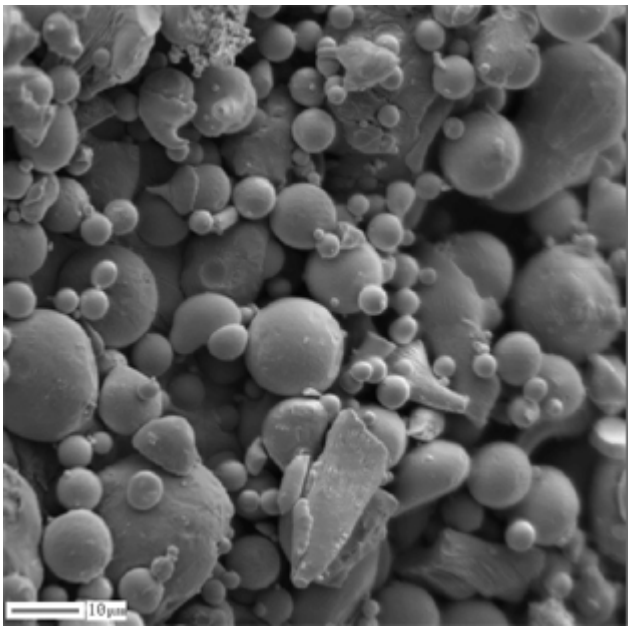

Figure 7. Representative results of scanning electron microscope analysis of fluorinated $Nd_2Fe_{14}B$-TiC powder showing no detectable surface damage from the coating process.

likely to permit ambient (air) powder handling and processing and a marked increase in bonded magnet environmental stability in drive motor applications.

To complete the series of technology development areas for improved bonded PM magnets, gas-atomized spherical magnet alloy powders have been subjected to bonding experiments using PPS as a high-temperature (melting point of about 300°C) polymer binder. Using desired test part dimensions and granulated PPS provided by MQI, a procedure was developed for dry blending and hot compression molding of cylindrical bonded magnets (diam = 9.5 mm, height = 9.5 mm). Magnet samples were molded from experimental $Nd_2Fe_{14}B$-TiC powder that was annealed and coated, and from commercial MQP-S-11-9 powder in an as-received condition. Two levels of loading, 50 and 60 vol%, were used, and the resulting bonded samples were sent to MQI for pulse magnetization and characterization to investigate the magnetic properties as a function of powder loading fraction. As shown in Figure 8, the data for the bonded MQI powder are a close match to the predicted curve, using a well-established value for the maximum energy product of the fully aligned and sintered magnet alloy. On the other hand, the data for the Ames experimental powder rest well above the predicted curve, perhaps reflecting uncertainty in the BH_{max} value of an optimum form of this alloy. Preliminary bonded magnet samples made from the experimental $YDyFe_{14}B$ powder were produced and sent for testing. Characterization results are not yet available. A polymer-assisted molding process with this new type of magnet alloy powder needs considerable development in collaboration with our industrial partner to extend the magnet powder loading fraction above 70% while maintaining suitable molding pressures for practical bonded magnet applications.

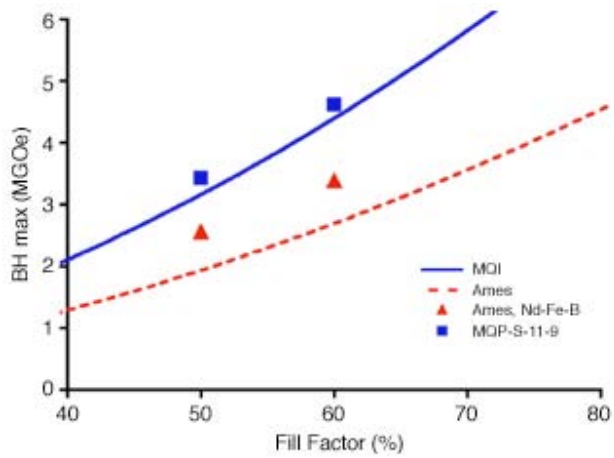

Figure 8. Comparison of PPS bonded magnet energy product data points to loading fraction prediction curves calculated from $[(BH)_{max}]^{bonded} = f^2(BH)_{max}$, where the MQI and Ames curves are based on $(BH)_{max}$ values of 11.1 and 6.8 MGOe, respectively.

Conclusions

Considerable progress on a novel alloy design approach for a PM compound with high-temperature magnetic stability has

produced a U.S. patent application. This new MRE–Fe-B family of 2-14-1 compounds has demonstrated increased coercivity with reduced temperature coefficients for remanence and coercivity, better for traction motor applications than the current commercial particulates or spherical powders for bonded magnets. A clear path forward for MRE–Fe-B alloy design was also identified to increase the remanence and energy product while maintaining superior temperature coefficient values. Initial gas atomization trials with MRE-Fe-B suggest that post-atomization annealing may not be needed to improve the magnetic properties of the spherical powders, potentially a significant processing simplification. The fluidized bed fluoride coating process appears to enhance air oxidation stability of both Nd-based and MRE-based 2-14-1 fine powders, perhaps producing a beneficial effect on powder handling during polymer processing and adding to bonded magnet service life. Bonded magnet samples also have been molded from a high-temperature polymer and the gas-atomized powders, and their magnetic properties have been characterized through a relationship with a major commercial supplier in the bonded magnet industry.

References

R. W. McCallum, K. W. Dennis, B. K. Lograsso, and I. E. Anderson, "Method of Making Bonded or Sintered Permanent Magnets," U.S. Patent 5,240,513, August 31, 1993.

I. E. Anderson, B. K. Lograsso, and R. L. Terpstra, "Environmentally Stable Reactive Alloy Powders and Method of Making Same," U.S. Patent 5,372,629, December 13, 1994.

R. W. McCallum, K. W. Dennis, B. K. Lograsso, and I. E. Anderson, "Method of Making Bonded or Sintered Permanent Magnets (continuation)," U.S. Patent 5,470,401, November 28, 1995.

I. E. Anderson and R. L. Terpstra, "Apparatus for Making Environmentally Stable Reactive Alloy Powders," U.S. Patent 5,589,199, December 31, 1996.

I. E. Anderson, B. K. Lograsso, and R. L. Terpstra, "Environmentally Stable Reactive Alloy Powders and Method of Making Same," U.S. Patent 5,811,187, September 22, 1998.

R. W. McCallum and D. J. Branagan, "Carbide/Nitride Grain Refined Rare Earth-Iron-Boron Permanent Magnet and Method of Making," U.S. Patent 5,803,992, September 8, 1998.

R. W. McCallum and D. J. Branagan, "Carbide/Nitride Grain Refined Rare Earth-Iron-Boron Permanent Magnet and Method of Making," U.S. Patent 5,486,240, January 23, 1996.

D. J. Branagan and R. W. McCallum, "The Effects of Ti, C, and TiC on the Crystallization of Amorphous $Nd_2Fe_{14}B$," *J. Alloys and Compds.*, **245** (1996).

D. J. Branagan, T. A. Hyde, C. H. Sellers, and R. W. McCallum, "Developing Rare Earth Permanent Magnet Alloys for Gas Atomization," *J. Phys. D: Appl. Phys.*, **29**, p. 2376 (1996).

M. J. Kramer, C. P. Li, K. W. Dennis, R. W. McCallum, C. H. Sellers, D. J. Branagan, L. H. Lewis, and J. Y. Wang, "Effect of TiC Additions to the Microstructure and Magnetic Properties of $Nd_{9.5}Fe_{84.5}B_6$ Melt-spun Ribbons," *J. Appl. Phys.*, **83**(11), pt. 2, p. 6631 (1998).

D. J. Branagan and R. W. McCallum, "Changes in Glass Formation and Glass Forming Ability of $Nd_2Fe_{14}B$ by the Addition of TiC," *J. Alloys and Compds.*, **244** (1–2), p. 40 (1996).

FY 2003 Publications/Presentations

M.J. Kramer, Y. Xu, K.W. Dennis, I. E. Anderson, and R.W. McCallum, "Development of Improved Powder for Bonded Permanent Magnets," *IEEE Transactions on Magnetics*, (in press, publication in September 2003).

I. E. Anderson, "Development of Improved Powder for Bonded Permanent

Magnets," presented at INTERMAG 2003, Boston, Massachusetts, April 2003.

I. E. Anderson, "Development of Powder Processing for Bonded Permanent Magnets," presented at PM^2TEC 2003, APMI/MPIF Annual Meeting, Las Vegas, Nevada, June 2003.

C. Carbon Foam for Electronics Cooling

Nidia C. Gallego, Beth Armstrong, April D. McMillan, and J. W. Klett
Oak Ridge National Laboratory
P.O. Box 2008, MS 6087, Bldg. 4508
Oak Ridge, TN 37831-6087
(865) 241-9459; fax: (865) 576-8424; e-mail: gallegonc@ornl.gov

B. E. Thompson and A. G. Straatman
University of Western Ontario,
London, Ontario, Canada

DOE Technology Development Manager: Rogelio Sullivan
(202) 586-8042; fax: (202) 586-1600; e-mail: rogelio.sullivan@ee.doe.gov
ORNL Technical Advisor: David P. Stinton
(865) 574-4556; fax: (865) 241-0411; e-mail: stintondp@ornl.gov

---

Contractor: Oak Ridge National Laboratory, Oak Ridge, Tennessee
Prime Contract No.: DE-AC05-00OR22725

Objectives

- Collaborate with automotive partner to develop carbon foam heat exchanger and heat sink designs that dissipate more than 30 W/cm^2 using standard cooling fluids.
- Develop a strategy to reduce the high cost of carbon foam.
- Determine the foam structure or morphology that results in optimum heat transfer for various thermal management applications.

Approach

- Study fundamental mechanisms of heat transfer in carbon foam and develop an engineering model that allows comparison of conventional and carbon foam heat exchangers.
- Develop a cost model that can be used to guide process development efforts to reduce the high cost of carbon foam.
- Build and operate a passive evaporative cooling system (PECS) to evaluate and compare the performance of carbon foam and diamond heat spreaders.

Accomplishments

- Developed a process cost model that indicates that the price of the pitch precursors and the time and temperature of the carbonization and graphitization cycles have the greatest influence on the cost of carbon foam.
- Developed an engineering model of heat flow through carbon foam that indicates that carbon foam heat exchangers failed to perform as expected because cooling air flowing over the foam failed to access the extensive surface area. This would suggest that designs that force air through the foam and not over the foam would perform much better.

- Proved high-conductivity carbon foam to be an excellent heat spreader when evaluated in the PECS system; it dissipated more than three times the amount of heat dissipated using state-of-the-art diamond heat spreaders.

Future Direction

- Conduct processing studies focused on finding alternative low-cost pitch precursor materials to replace the current raw materials and therefore reduce the cost of carbon foam.
- Modify the structure or morphology of the carbon foam for optimum heat transfer. Modeling results indicate that more open, less dense structures with easily accessible porosity would increase the heat transfer.
- Operate the PECS using carbon foam heat spreaders with more open, less dense structures.

Introduction

Many improved electronic components introduced in recent decades, such as higher-power computer chips and power converters, generate significantly more heat and require more efficient devices for dissipating that heat. Many techniques have been explored to improve the efficiency of heat transfer devices, such as micro-channels, heat pipes, and other exotic designs; however, none has been able to adequately cool the electronics. These devices must incorporate very effective heat spreaders into the design of the heat sink to prevent localized hot spots and ensure that the temperature of the electronics does not exceed 125°C.

The high-conductivity carbon foam developed at Oak Ridge National Laboratory (ORNL) is an open-cell structure with highly aligned graphitic ligaments (see Figure 1); studies have shown the typical interlayer spacing (d002) to be 0.3356 nm, very near that of perfect graphite (0.3354 nm). As a result of its near-perfect structure, thermal conductivities along the ligament are calculated to be approximately 1700 W/m•K, with bulk conductivities = 180 W/m•K. Furthermore, the material exhibits low densities (0.25 to 0.6 g/cm^3) so that the specific thermal conductivity is approximately four to five times greater than that of copper. The high conductivity combined with the very high surface area (20,000 m^2/m^3) results in overall heat transfer coefficients for foam-based heat exchangers that are up to two orders of magnitude greater than those of conventional heat exchangers. As a result, foam-based heat exchangers or heat sinks could be dramatically smaller and lighter than conventional ones.

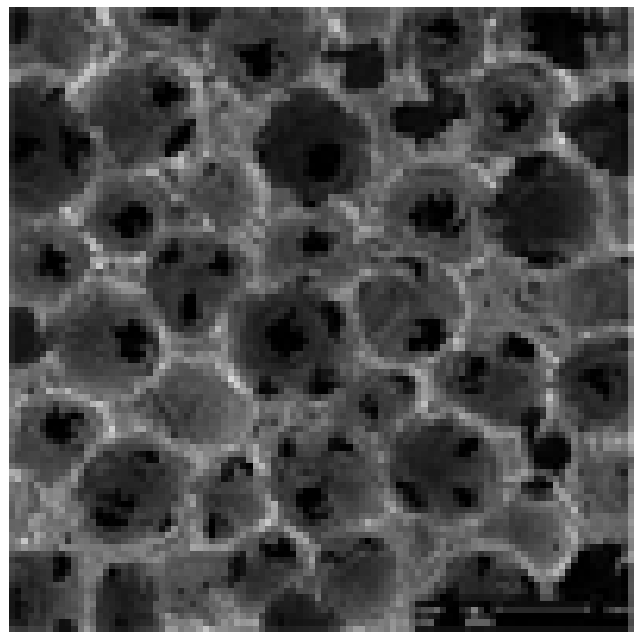

Figure 1. Graphite foam material developed at ORNL.

Automotive and industry partners are very concerned about the high cost of high-conductivity carbon foam. They are convinced that the cost of carbon foam must be reduced significantly before it can be used in most automotive applications. Work was

initiated during FY 2003 to determine what factors have the greatest impact on the cost of the foam. Once those factors have been identified, research efforts will be redirected to those areas.

Results

Cost Modeling of Carbon Foam

A detailed process economic model was constructed of the ORNL high-thermal-conductivity carbon foam manufacturing process.[1] The Excel-based model included the effects of 146 input variables on the expected sales price and manufacturing cost of this material. It also provides estimates of the capital investment, plant size, and employee level required. A set of values of the input variables was established as a baseline case, using data supplied by ORNL or obtained from industrial sources and potential suppliers. The results of the baseline case were analyzed to determine the most significant cost drivers (see Figure 2) and the sensitivity of results to these cost drivers. A set of advanced model analysis tools was used to visualize the relative magnitude of these drivers and their potential effect on product price. Risk analysis showed the probability of deviation from the expected product price. Another analysis provided insight into the sensitivity of results to production volume. From these results and analyses, we can provide the following results, which are based on high production volumes.

Assuming that major variables are close to the baseline values, the price of carbon foam at a production rate of 44,000 parts (2×3×1.5 in.) per week will be approximately \$4.95/piece (\$0.55/in.^{3}), with a manufacturing-only cost of \$2.97/piece (\$0.33/ in.^{3}).

This level of production will require a capital investment for equipment of approximately \$9.25 million and will require about 8400 ft^2 of manufacturing space, 29 technicians/operators, and 3 engineers.

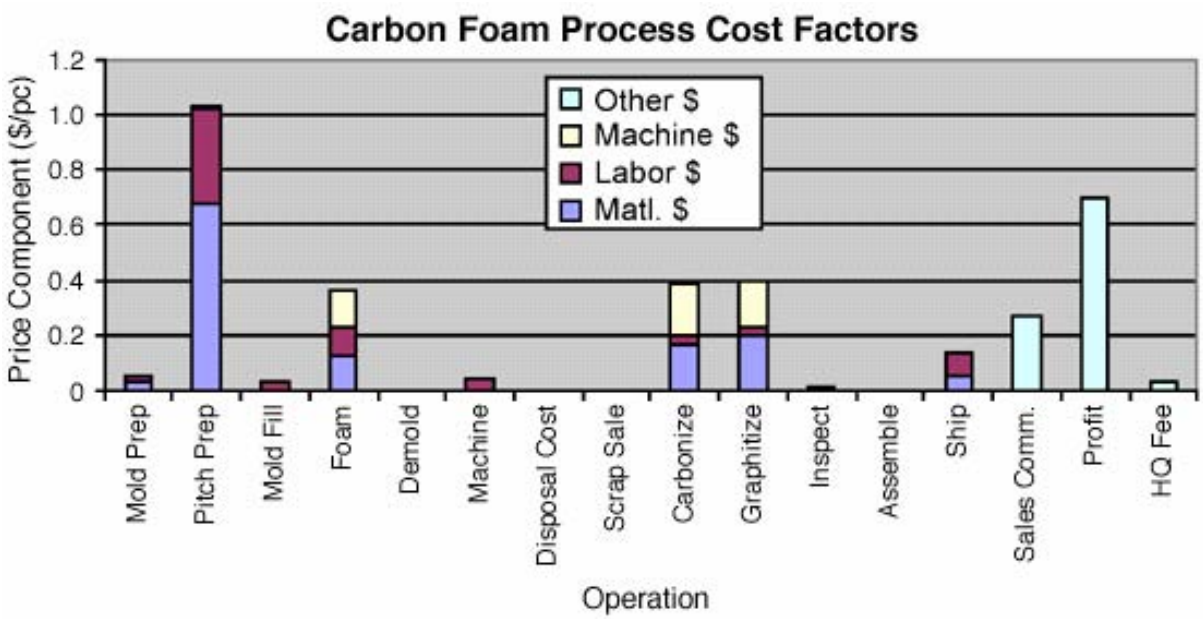

Figure 2. Carbon foam process cost factors.

The density of the foam product has the greatest influence on product price, on the basis of price per cubic inch. This result is apparently caused by the strong influence of amount of pitch required per volume of foam and the high sensitivity of foam price to pitch price.

Pitch price has the next greatest influence on foam price. Price could vary from \$0.45/in.^{3} to \$0.68/in.^{3} as the pitch price varies from \$3 to \$8/lb. The pitch raw material accounts for 24% of the sale price of foam (see Figure 3).

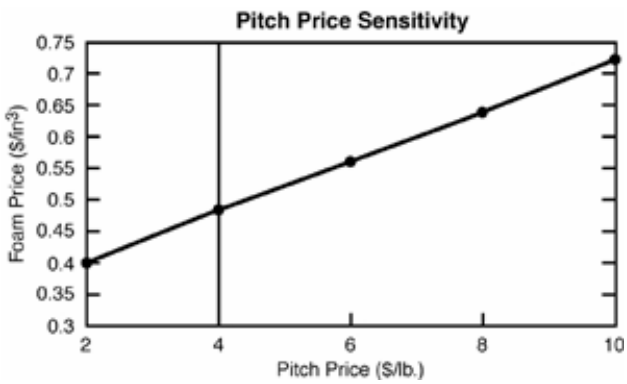

Figure 3. Correlation of the cost of the pitch precursor and the cost of carbon foam.

After business costs such as profit and sales cost, the three furnace operations are the next most important cost drivers. The carbonization and graphitization times and temperatures need to be reduced to minimize cost.

Modeling of Porous Carbon Foam Heat Exchangers

An engineering model[2] was developed that provides values for the thermal resistance and pressure drop in air-water heat exchangers with plate-fin and annular-fin configurations, based on a combination of the following:

- measurements of bulk conductivity of porous carbon foam
- well-established correlations for convective heat transfer from tubes, plates, and fins
- measured thermal resistance at the interface between aluminum and porous carbon foam with a number of different joints
- an engineering approximation for the effects of porosity on convective heat transfer

The model was compared both with available measurements obtained with conventional aluminum heat exchangers and with copycat heat exchangers made from carbon foam. Agreements between calculated and measured values of the heat transfer coefficient and pressure drop were sensible and within about 15% and 10%, respectively, which is adequate for typical design needs in thermal engineering.

The model suggests that finned carbon foam heat exchangers failed to perform as expected because the air flowing over the carbon foam failed to access the extensive surface area. If radiator designs could be developed that effectively use the surface area, 20 to 60% improvements over optimum aluminum-finned heat exchangers could be achieved. Note that the performance of a carbon foam heat exchanger is controlled more by the surface area accessed than by the high conductivity of the foam. This suggests that the porosity, pore density, dendrite structure, and strength of the carbon foam should be optimized simultaneously to enhance heat transfer with minimal increase in pressure losses.

It may not be possible to access sufficient surface area of carbon foam in conventional finned heat exchanger designs. This would suggest that designs that force air through the foam, and not over the foam, may be required. The structure of the foam would act like the fins of conventional heat exchangers. These designs would use all of the available surface area because the structure of the foam would act as the "fins."

In a cost model developed recently, the development of less-expensive pitch precursors was found to have the most dramatic effect on the cost of the carbon foam. Low-cost precursors have not been pursued in the past because we were concerned that the thermal conductivity would be negatively impacted. The engineering model was exercised to determine the significance of the thermal conductivity of the carbon foam for the performance of radiators. It was quite surprising to learn that a 25 to 50% reduction in thermal conductivity had only a minor effect (~5%) on the performance of the heat exchangers.

Passive Evaporative Cooling

A PECS was built in FY 2003 and operated extensively at ORNL. A simple schematic illustrating the concept is shown in Figure 4. A more thorough description of the operation of the system is included in article 2D, "Evaporative Cooling of Power Electronics" in this annual report. Similar systems developed by the National Security Agency that contained a limited-surface-area diamond heat spreader were able to achieve a power density of 28 W/cm^2 and were considered to be state-of-the-art technology. The system that was operated at ORNL with a graphite foam heat spreader was able to achieve a power density of over 120 W/cm^2, more than four times the power density attained using the diamond heat spreader. The graphite foam has proved to be an excellent heat spreader because of the extensive surface area, the very high thermal conductivity, and the fact that the foam is easily wetted by the evaporative coolants.

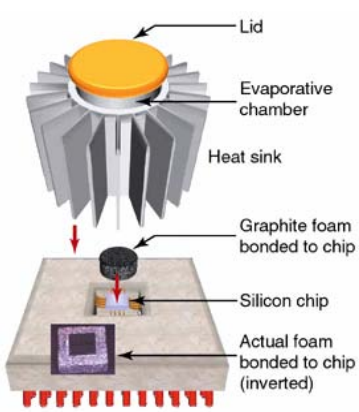

Figure 4. Schematic diagram of the evaporative cooling system.

Conclusions

A process cost model was developed that evaluated the effect of more than 100 variables on the cost of carbon foam. The model indicates that the price of the pitch precursors and the time and temperature of the carbonization and graphitization cycles have the greatest influence on the cost of carbon foam. An engineering model of heat flow through carbon foam was also developed that indicates that carbon foam heat exchangers failed to perform as expected because cooling air flowing over the foam failed to access the extensive surface area. Additional research is needed to understand the relationship between material structure and heat transfer. Findings suggested that more-porous, less-dense foams would recruit additional surface area—provided, of course, that the carbon structure has adequate strength. The capability to control pore density (pores per inch) and to maintain an open pore structure (percentage of open pores) is important if the benefits of the porous surface structure are to be realized in practical applications. Finally, carbon foam proved to be a very effective heat spreader when used in an evaporative cooling system. The carbon foam heat spreader was able to dissipate more than four times as much heat as the previously used diamond heat spreader.

References

1. E. H. Kraft, *Process Economic Model for High Thermal Conductivity Carbon Foam, Final Report*, June 4, 2003.

2. B. E. Thompson, A. G. Straatman, R. Culham, M. Yovanovich, A. G. Hunt, Q. Yu, and P. Oosthuisen, *Modeling of Porous-Carbon-Foam Heat Exchangers*, February 28, 2003.

FY 2003 Publications/Presentations

N. C. Gallego and J. W. Klett, "Carbon Foams for Thermal Management", presented at the International Seminar: Advanced Applications for Carbon Materials, Jeju, Korea, September 12–13, 2002 (to be published in the proceedings).

N. C. Gallego and J. W. Klett, "Carbon Foams for Thermal Management," *Carbon* 41 (2003) 1461–1466.

N. C. Gallego, J. W. Klett, and A. D. McMillan, "Effect of Processing Conditions on Properties of Graphite Foams," presented at Carbon '02: An International Conference on Carbon, Beijing, China, September 15–19, 2002 (to be published in the proceedings).

N. C. Gallego, A. D. McMillan, and S. K. Stinton, "Effect of Heat Treatment on the Rheological Properties of Mesophase Pitch and Final Properties of Carbon Foam," presented at Carbon '03: An International Conference on Carbon, Oviedo, Spain, July 6–10, 2003 (to be published in the proceedings).

N. C. Gallego, T. D. Burchell, and J. W. Klett, "Neutron Irradiation Damage in Graphite Foam and Its Effect on Properties," presented at Carbon '03: An International Conference on Carbon, Oviedo, Spain, July 6–10, 2003 (to be published in the proceedings).

D. Evaporative Cooling of Power Electronics

R. D. Ott, B. L. Armstrong, A. D. McMillan, C. A. Walls
Oak Ridge National Laboratory
P.O. Box 2008, MS 6083, Bldg. 4508
Oak Ridge, TN 37831-6083
(865) 574-5172; fax: (865) 574-4357; e-mail: ottr@ornl.gov

DOE Technology Development Manager: Nancy Garland
(202) 586-5673; fax: (202) 586-9811; e-mail: nancy.garland@ee.doe.gov
ORNL Technical Advisor: David Stinton
(865) 574-4556; fax: (865) 574-6918; e-mail: stintondp@ornl.gov

---

Contractor: Oak Ridge National Laboratory, Oak Ridge, Tennessee
Prime Contract No.: DE-AC05-00OR22725

Objectives

- Identify methods of utilizing carbon (graphite) foam for passive evaporative cooling of power electronics.
- Study the durability of graphite foam under environmental conditions similar to those of various applications.
- Design and build a prototype evaporative chamber for testing different methodologies for evaporative cooling.

Approach

- Construct test chamber with a hollow cavity for evaporative fluid and vapor.
- Conduct tests with the unit, with either chilled water or air as a cooling medium, to regulate variables to determine the effectiveness of the cooling system.
- Measure the durability of the graphite foam for thermal stability and compressive stress, corrosion, erosion, vibration, and salt fog resistance. Construct and conduct the appropriate tests for each of the six durability areas.

Accomplishments

- Determined that pool boiling and thin film evaporation are effective methodologies for use of graphite foam for evaporative cooling.
- Demonstrated power dissipations of up to 1500 W at temperatures of up to 100°C.
- Found no effect of thermal cycling over a ΔT of 60–75°C and 100,000 cycles on the durability of graphite foam. In addition, no decrease in compressive stress or modulus resulted after cycling.
- Found that the foam structure itself is unaffected by exposure to a mixture of propylene glycol and water (Zerex™) at room temperature, 60°C, and 100°C for up to 1000 hours. However, the mechanical integrity of the solder attaching the foam to the substrate is a valid concern.

Future Direction

- Combine this research project in FY 2004 with the project "Carbon Foam for Electronics Cooling."

Introduction

A novel technique for creating pitch-based carbon foam was developed at Oak Ridge National Laboratory (ORNL)[1,2] before 1997. This technique uses mesophase pitch as a starting material but does not require the costly blowing or stabilization steps that typical carbon foams require.[3] The ORNL foam is an open-cell structure with highly aligned graphitic ligaments; studies have shown the typical interlayer spacing (d002) to be 0.3356 nm, very near that of perfect graphite (0.3354 nm). Because of its near-perfect structure, thermal conductivities along the ligament are calculated to be approximately 1700 W/m·K, with bulk conductivities 180 W/m·K. Furthermore, the material exhibits low densities (0.25–0.6 g/cm^3) such that the specific thermal conductivity is approximately four to five times greater than that of copper. The very high surface area (20,000 m^2/m^3) combined with the high thermal conductivity suggests that graphite foam has significant potential for application as a thermal management material.

One potential application of graphite foam as a thermal management material is in the area of cooling integrated circuit chips (ICCs). Current electronic ICCs, similar to power electronic integrated gate bipolar transistors used to control voltages in hybrid vehicles, are placed printed-side-up in a ceramic package with "over-the-top" wire bonds. Unfortunately, this design is not suited for significant heat dissipation through the top of the package to a standard heat sink, as there is an insulating air gap between the silicon chip and the ceramic package. A new concept being developed is the "flip-chip" design, in which the silicon chip is inverted and the back of the printed chip is oriented toward the top of the package. In this case, it is simple to join a heat spreader directly to the silicon chip and immerse it in an evaporative cooling fluid (i.e., fluoro-carbon). In the process, the latent heat of vaporization removes significantly more heat than the sensible heat change of the fluid and transfers it very efficiently to the fins of the heat sink.

The limitations of this design are the surface area and thermal conductivity of the spreader mounted to the back of the chip. Current state-of-the-art spreaders are polycrystalline diamond wafers with thermal conductivities of up to 1600 W/m·K (more than four times that of copper). As a result of the limited surface area of the diamond spreader, the maximum power density achieved without overheating the system is 28 W/cm^2. When the diamond spreader is replaced with graphite foam, a power density of 100 W/cm^2 is attained without overheating the system. Theoretically, significantly higher power densities can be attained with proper design and fluid content. If this concept could be applied to power electronics, the benefit would be substantial in reducing temperatures, increasing reliability, and possibly reducing costs.

One issue of importance with regard to the performance of the ORNL foam is its durability under typical operating conditions. It is hoped that once we understand how the foam behaves in environments approximating actual operating parameters, it can be modified as necessary to meet application-specific needs. To this end, several durability studies have been undertaken, the constraints directed by either the Energy Efficiency Tech Team or by industrial partners. The studies include thermal cycling, compression testing, corrosion, erosion, vibration, and salt spray (fog).

Approach

The use of a passive evaporative cooling system (PECS) would be advantageous in ICC applications to minimize pressurized systems and limit the weight and size of existing spray cooling systems. Most PECSs are characterized by pool boiling or thin film evaporation modes. The high thermal conductivity and surface area of the graphite foam lends itself well to these applications, but demonstration of its feasibility was required. A PECS was constructed based on a hollow aluminum chamber with graphite foam mounted onto a heater plate. An evaporative fluid (evaporant) will be added to the system, and the heat flux will be measured as a function of heat added to the system.

Six sets of durability experiments will be carried out in the areas of thermal stability and compressive stress, corrosion, erosion, vibration, and salt spray (fog) exposure. The thermal conductivity and compressive stress change will be measured as a result of thermal exposure (ΔT of 60–75°C and 100,000 cycles at 5 gal/min). Thermal conductivity and joint integrity will be measured and examined as a result of 1000-hour exposures in 50% propylene glycol/50% water mixture at room temperature, 60°C, and 100°C. Mass loss will be measured after exposure to 1600 ft/min airflow. Thermal conductivity and structural integrity will be measured and examined after vibration conditions of 7 g and 10–20 Hz for 40 hours. Mass change and thermal conductivity will be measured after exposure to salt fog [modified standard Society of Automotive Engineers (SAE) J12111 and SAE J726].

Results

The PECS was built and evaluated as an appropriate methodology for testing the heat dissipative capability of graphite foam in ICC applications. A simple schematic illustrating the concept of the PECS is shown in Figure 1. The PECS is hollow and contains an evaporator (graphite foam) and a working fluid at a reduced pressure equal to the vapor pressure of the fluid at room temperature. Heat is added to the bottom of the PECS, passes through the metal base plate (Figure 1), and is then transferred to the graphite foam through a soldered or brazed joint. The extremely high ligament thermal conductivity of the foam (equivalent to that of diamond) rapidly transmits the heat to all the internal surfaces of the foam. Concurrently, capillary action wicks the working fluid into the foam and coats the internal surfaces. After all the permanent gases are removed (gases that do not condense, such as oxygen or nitrogen), any heat that is added to the system disturbs the equilibrium, and the working fluid evaporates (or boils). The vapor then condenses on a wall of the chamber that is cooled externally (typically with air).

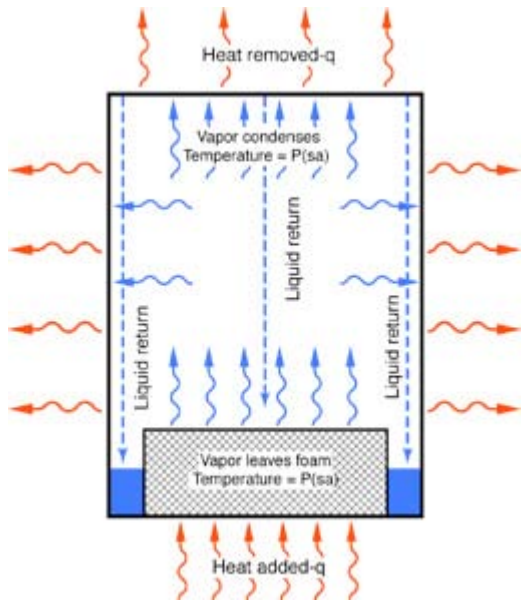

Figure 1. Schematic diagram of the evaporative cooling system.

The advantage of the graphite foam is that its extremely high surface area results in dramatically higher heat fluxes that can be transmitted to the working fluid uniformly. This aspect of the project was conducted in collaboration with another project, "Advanced Cooling for Naval Radars," which was funded by Office of Naval Research. The feasibility of pool boiling and of the PECS

was demonstrated using a chip provided by the National Security Agency (NSA) as the heater core in a flip-chip design configuration. Power dissipations of up to 1300 W at temperatures of up to 100°C were demonstrated (Figure 2). The feasibility of using graphite foam as a heat spreader to prevent hot spots on a chip or dissipate high heat fluxes was demonstrated.

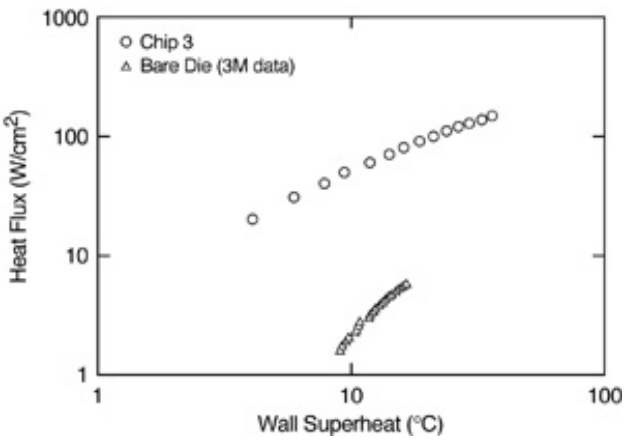

Figure 2. Heat flux results of a PECS test using an NSA chip and graphite foam as the heat spreader.

Several durability tests were performed to determine the graphite foam's ability to withstand corrosion, thermal cycling, vibration, erosion, and salt spray (fog). Each test was conducted following ASTM standards or a modification of a standard, and the work is still ongoing in order to establish a database of durability information. The durability tests were also conducted in collaboration with another DOE project, "Carbon Foam for Electronics Cooling." A milestone report[3] entitled *Durability of Graphite Foam: Effects of Thermal Cycling, Compression, Corrosion, Erosion, Vibration, and Salt Fog* was completed in June 2003. The procedures and detailed results from the durability tests can be found in the milestone report. Some of the significant data and conclusions are described in the following paragraphs.

Thermal cycling tests were performed in an infrared furnace that allowed the temperature to be rapidly cycled from room temperature to 110°C in a matter of minutes. After more than 42,000 thermal cycles, there was no statistically significant change in compressive stress[4] or compressive modulus (see Figure 3.)

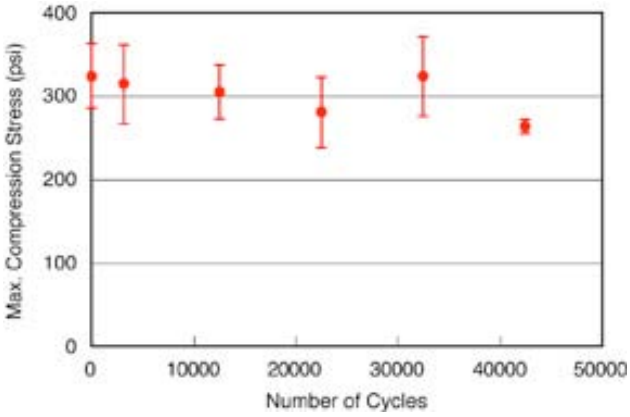

Figure 3. Graphite foam thermal cycling compression test results: maximum compression stress.

To address the concern that the graphite foam might become corroded in applications where it is in direct contact with an evaporant or coolant, a study was completed to determine if the foam structure and conductivity, or the reliability of the braze or weld that joins the foam to the support material, was altered after exposure. Samples of graphite foam were exposed to a 50% propylene glycol/50% water mixture (Zerex) for up to 1000 hours at room temperature, 60°C and 100°C.[5] The study samples consisted of a series of treated and untreated foam blocks bonded to aluminum, copper, brass, and stainless steel plates using 50/50 (tin/lead) solder. From this initial study, it was evident that the foam structure itself is unaffected by exposure to Zerex at temperatures of up to 100°C after 1000 hours (Figure 4). However, the mechanical integrity of the solder attaching the substrate (metal plate) to the foam was affected, especially at the 100°C condition.

Erosion tests were carried out on graphite foam samples (1-in. cube with a 0.25-in. hole machined through the center) to measure the

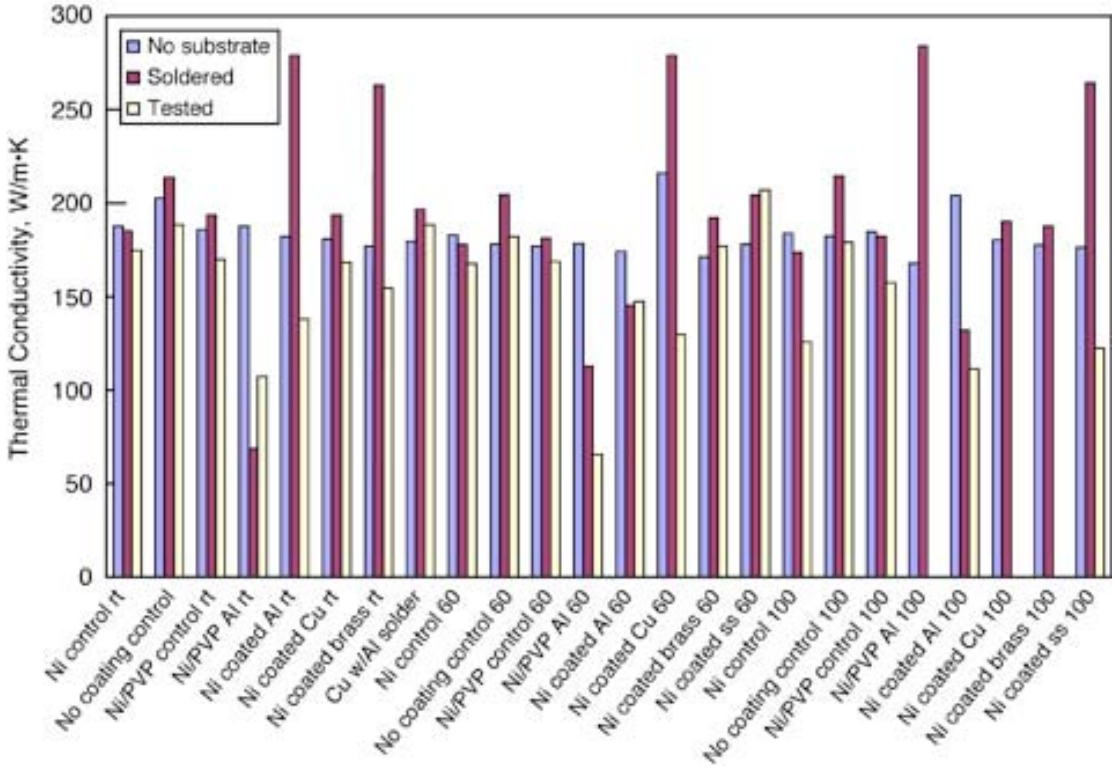

Figure 4. Effects of corrosion on thermal conductivity after 1000 hours in Zerex solution at room temperature, 60°C, and 100°C.

mass loss and mass loss rate at a given impinging air velocity. Air was blown onto the graphite foam cubes at a face velocity of approximately 1600 ft/min for 5 min. The mass loss rate of uncoated and coated carbon foam exceeded the design limits set by the industrial partners directing this test set. Thus the graphite foam would not be acceptable for applications subject to impinging airflow.

Vibration testing was conducted to identify any degradation of the graphite foam or the interface of a foam mounted to a metallic substrate. Thermal conductivity before and after testing was used as the measure of degradation. None of the 18 foam samples tested showed any visual degradation or physical debonding from the substrates. Thermal conductivity measurements were identical before and after testing, indicating no degradation of either the foam structure or the bond between the foam and substrate.

Conclusions

A PECS was built and operated extensively in FY 2003. The performance of the system operated using a diamond heat spreader was compared with the performance of a graphite foam heat spreader. The system operating with the graphite foam heat spreader proved to be far superior and dissipated more than three times as much heat as the diamond heat spreader. The total heat transfer of approximately 1500 W at temperatures of less than 60°C on the substrate demonstrates that graphite foam is a viable material as a heat dissipater or heat spreader for power electronics applications. The capability to use a PECS will enable applications in automotive markets where weight is a concern.

The durability tests showed that graphite foam could withstand several conditions, such as thermal cycling and salt fog exposure, without degradation of the structure or its properties. Since graphite foam has a very low compressive modulus (0.08–0.114 GPa)

compared with other materials commonly used as heat sinks or spreaders, such as aluminum (70 GPa), it is anticipated that the foam will be highly shock resistant. The data from the thermal cycling and compression testing indicate the same conclusion. The corrosion tests revealed that the foam structure itself was unaffected by the exposure to the Zerex solution even at 100°C. However, issues related to the bonding of the graphite foam to metallic substrates were raised as a concern, indicating that the selection of the solder relative to the substrate (heat exchanger or base plate) will be important. The erosion tests revealed that the foam erosion rate was too high for applications subject to impinging airflow. There was no evidence that the vibration testing produced an effect on the thermal properties or the bonding interface that would limit its use in automotive applications.

References

1. J. Klett, "High Thermal Conductivity, Mesophase Pitch-Derived Carbon Foam," in *Proceedings of the 1998 43rd International SAMPE Symposium and Exhibition, Part 1 (of 2)*, Anaheim, California, 1998.

2. J. Klett, "High Thermal Conductivity, Mesophase Pitch-Derived Carbon Foams," *Journal of Composites in Manufacturing*, **15**(4), 1–7 (1999).

3. B. L. Armstrong, A. McMillan, N. Gallego, R. Ott, M. Trammell, and C. Walls, *Durability of Graphite Foam: Effects of Thermal Cycling, Compression, Corrosion, Erosion, Vibration, and Salt Fog*, Letter Report, Oak Ridge National Laboratory, July 2003.

4. American Society of Testing and Materials C695, *Standard Test Method for Compressive Strength of Carbon and Graphite*, 2000.

5. Society of Automotive Engineers J12111, *Recommended Environment Practices for Electronic Equipment*, 1978.

FY 2003 Publications/Presentations

N. C. Gallego and J. W. Klett, "Carbon Foams for Thermal Management," *Carbon* **41** (2003) 1461–1466.

N. C. Gallego and J. W. Klett, "Carbon Foams for Thermal Management," presented at International Seminar: Advanced Applications for Carbon Materials, Jeju, Korea, September 12–13, 2002 (to be published in the proceedings).

N. C. Gallego, J. W. Klett and A. D. McMillan, "Effect of Processing Conditions on Properties of Graphite Foams," presented at Carbon '02: An International Conference on Carbon, Beijing, China, September 15–19, 2002 (to be published in the proceedings).

E. High-Temperature Film Capacitors

B. A. Tuttle, G. Jamison, D. Wheeler, J. S. Wheeler, and D. Dimos
Sandia National Laboratories
P.O. Box 5800, MS 1411
Albuquerque, NM 87185-1405
(505) 845-8026, fax: (505) 844-2974

DOE Program Managers: Susan Rogers
(202) 586-3976; fax((202) 586-9811; e-mail: susan.rogers@ee.doe.gov
Rogelio Sullivan
(202) 586-8042; fax (202) 586-1600; e-mail: rogelio.sullivan@ee.doe.gov
Graham Hagey
(202) 256-2457; e-mail: graham.hagey@hq.doe.gov

Contractor: Sandia National Laboratories, Albuquerque, New Mexico
Prime Contract No.: 04-94AL85000

Objectives

- Develop a replacement technology for aluminum electrolytic dc bus capacitors currently used for fuel cell/electric hybrid vehicles.
- Develop a high-temperature polymer dielectric film technology that has dielectric properties technically superior to those of aluminum electrolytic dc bus capacitors and that is of comparable or smaller size.
- Scale up cost-competitive polymer film dielectric technology.
- Develop high-volume production process for dielectric film roll fabrication.
- Fabricate prototype capacitors.

Approach

- Contact automobile design and component engineers, dielectric powder and polymer film suppliers, and capacitor manufacturers to determine state-of-the-art capabilities and to define market-enabling technical goals.
- Develop a project plan with automobile manufacturers and large and small capacitor companies to fabricate polymer dielectric sheets suitable for FreedomCAR capacitor manufacturing.
- Synthesize unique conjugated polyaromatic chemical solution precursors that result in dielectric films with low dissipation factors (DFs) and excellent high-temperature dielectric properties.
- Develop polymer film processes and technologies that will lower costs to permit competitive high-volume capacitor manufacturing.
- Interact with Oak Ridge National Laboratory (ORNL) with regard to mechanical characterization of films.

Accomplishments

- Invented chemical synthesis procedures that resulted in polymer films with four times the energy density of commercial polyphenylene sulfide (PPS) at 110°C. Scaled-up hydroxylated polystyrene (PVOH) films exhibited dielectric constants of 4.7 and DFs of 0.009 at temperatures of up to 110°C, thus meeting technical requirements for commercialization.
- Collaborated with TPL, Inc., and Steiner Corporation to adjust high-volume metallization procedures for Sandia National Laboratories (SNL) 10-in.-wide, 450-ft-long dielectric film.
- Initiated a project to investigate the effects of three different cross-linker species and their concentrations on the dielectric and mechanical properties of SNL PVOH films. This effort would permit fabrication of wound capacitors by high-volume metallization processing.
- Collaborated with ORNL to characterize mechanical properties of PVOH films.

Future Direction

- Perform extensive electric field and temperature characterization to determine that SNL polyfilm dielectrics will meet FreedomCAR requirements for breakdown field and DF for temperatures from –40 to 110°C.
- Fabricate and characterize 1-µF wound capacitors using non-high-volume metallization techniques to determine if they will meet General Motors (GM) requirements. Supply capacitors to GM, Ford, and Chrysler for testing in inverter-type environments.
- Have large-value (20- to 200-µF) capacitors fabricated by vendor(s) evaluated by GM and SNL in simulated electric hybrid vehicle environments.
- Develop chemical synthesis procedures for high-performance, more cost-effective films.

Results

Strategy and Interactions

SNL has actively interacted with a number of representatives from the automobile industry to obtain their perspective on what is needed for 2004 automobiles. In FY 2003, SNL continued its emphasis on the development of polymer film dielectrics for two reasons. First, GM has been adamant about soft breakdown dielectric film technology—a phenomenon that bulk ceramic capacitors do not exhibit. Second, emphasis on polymer dielectrics provides greater balance of the DOE effort between polyfilm and ceramic technologies, as requested by the Electrical and Electronics Tech Team. SNL has developed a close working relationship with the Advanced Technology Vehicles Division of GM. Based on phone calls and e-mail exchanges with GM staff that outlined technical progress and component qualification procedures, SNL has modified project plans for the development of polymer film dielectrics for FreedomCAR applications.

These interactions led us to the conclusion that the most viable replacement technology for electrolytic dc bus capacitors by 2004 is multilayer polymer film capacitors. Reducing the size of the polymer capacitors was most often cited by automobile design engineers and capacitor manufacturers as a needed technology-enabling breakthrough. In addition, it is necessary to improve high-temperature (110°C) performance while keeping the technology cost-competitive. For polymer film dielectrics, based on the GM 2004 criteria for capacitance density of 2.0 µF/cm^3, the team agreed that if a polyfilm of K = 4.5 could be developed that met the operating temperature requirements, then that film would be suitable for scale-up.

Based on the criteria from GM, an individual dielectric layer thickness of approximately 3 µm for polyfilm capacitors is projected. These thickness values are based on operating field strengths of 2 MV/cm for the newly developed polyfilm capacitors. Based on these assumptions and on measurement of presently available commercial capacitors, size comparisons and capacitance densities were obtained for 500 µF dc bus capacitors for different technologies. Soft breakdown behavior and lower cost are assets for polymer film capacitors. The projected polymer film capacitor volume was calculated assuming that there is 40% non-active capacitor space and 200-nm thick electrodes are used. Note that the volumetric capacitance efficiency for a K = 4.5 polyfilm capacitor of 2.4 µF/cm^3 exceeds the near-term commercialization goal of 2 µF/cm^3.

Polymer Film Dielectric Development

SNL polymer film dielectric development has been based on the request from manufacturers that the new polyfilm dielectrics have voltage and temperature stability equivalent to that of present PPS technology. Thus a structural family of polymer dielectrics has been designed and synthesized to meet two of the most stringent FreedomCAR requirements: (1) low dielectric loss and (2) extremely good temperature stability. A patent disclosure has been initiated covering the design and synthesis techniques for this polymeric family. A further criterion for wound capacitors is that PVOH films can be adequately released from underlying carriers without tearing. In FY 20O3, we investigated three different cross-linker species at four different concentration levels in an attempt to enhance the ductility of our PVOH-based polymer. Our baseline cross-linker species was VEctomer 4010 at the 30 wt% level. Figure 1 shows schematic diagrams of the three different types of cross-linkers evaluated, VEctomer 4010 and 5015 and tetraethylene glycol divinyl ether (TEGDE). Structurally, these cross-linkers varied in the amount of rigid benzene cores and the density of vinyl ether termini.

PVOH films were synthesized using MEK solvent—similar to that used for casting at Brady Corporation of Milwaukee. Concentrations of 5, 15, 20, and 30 wt% were investigated. It is encouraging that we were able to synthesize films that had reasonable dielectric loss at low cross-link addition levels. Based on the work of Wereszczak, films with less than 30 wt% cross-linker have slightly lower hardness and elastic modulus. An example of low dielectric loss (low DF) with low cross-link density is shown in Figure 2 for VEctomer 5015 cross-linker. The dielectric constant and DF were measured at 1 kHz and 25°C in Figure 2. DFs of 0.005 were measured for the 5 wt% cross-linker addition at 110°C as well as for the 25°C measurements shown. Breakdown strengths appeared quite reasonable, in the 2.2 to 4.2 MV/cm range, for these spin-deposited films of approximately 0.5 µm in thickness on aluminum-coated silicon wafers. These measurements were made

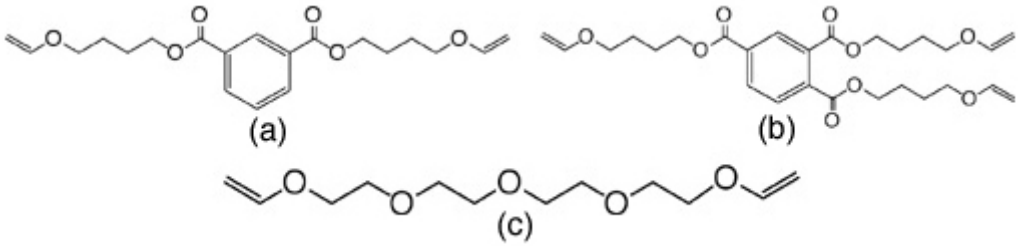

Figure 1. Schematic diagrams of three different cross-linkers: (a) VEctomer 4010, (b) VEctomer 5015, and (c) TEGDE

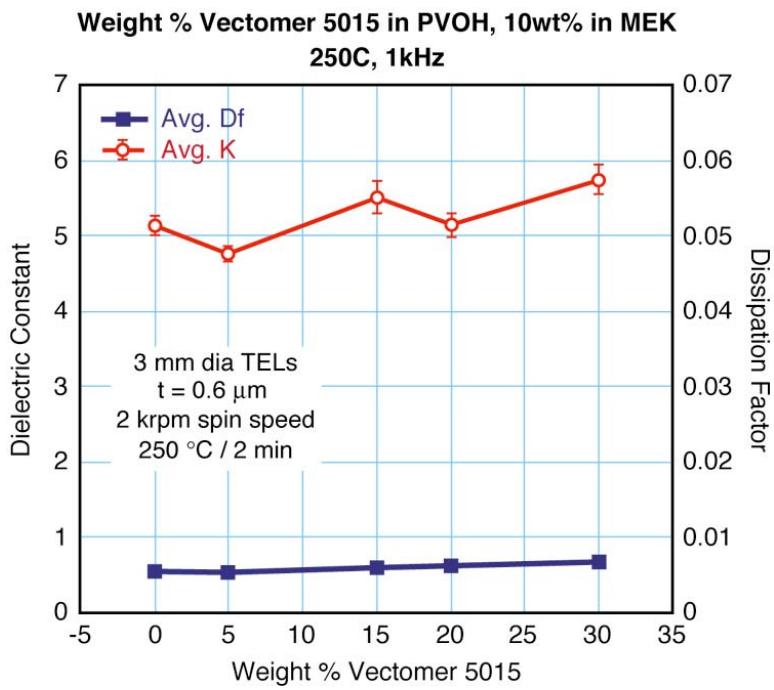

Figure 2. Dielectric constant and dissipation factor of SNL hydroxylated polystyrene film as a function of VEctomer 5015 cross-linker concentration.

using 3-mm-diam gold electrodes. Based on mechanical property data, we will select one of the lower (less than 30 wt%) cross-link concentration films for scale-up at Brady Corporation.

Figure 3 is a pictorial view of our PVOH film scale-up activities in FY 2003. Continuous slot-die-cast PVOH polymer film sheet is shown in Figure 3(a). The PVOH film sheets deposited on mylar carriers range from 20 to 50 ft in length. The 10-in.-wide film roll is then slit to 2-in. width for capacitor winding. We worked with TPL of Albuquerque to fabricate these slit rolls. Development of technology that was more amenable to high-volume production required interaction with Brady Corporation. We were able to cast 450-ft lengths of 10-in.-wide polymer film using the Brady prototype caster on 6-in.-diam mandrills. A high-volume electrode deposition process step is essential to manufacturing large-value capacitors with good volumetric efficiency. Steiner Corporation deposited aluminum electrodes on SNL films by a proprietary high-volume manufacturing process. The slit film roll electroded by Steiner is shown in Figure 3b. Because our polymer film tore during winding, the cure temperature of the PVOH film was decreased and the Steiner process was modified. Two wound polymer film capacitors of the modified process are shown in Figure 3c. Silver epoxy terminations were used after the zinc flame spray termination process was unsuccessful. Our dielectric film thickness is presently 4 to 5 µm for these capacitors.

Summary

Critical economic and technical issues for improvement of dc bus capacitors for FreedomCAR vehicles were determined through discussions and visitations with automobile design engineers, chemical synthesis companies, and capacitor manufacturers. PVOH film dielectric development was emphasized in FY 2003, and we have developed a multi-step project

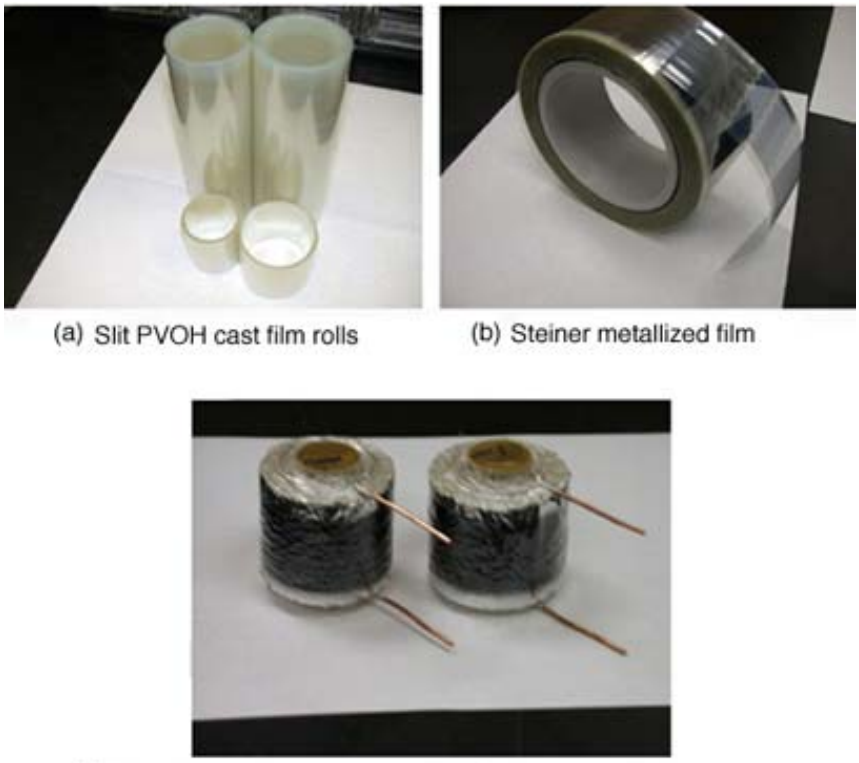

(a) Slit PVOH cast film rolls (b) Steiner metallized film

(c) Wound capacitors using modified Steiner metallization process

Figure 3. SNL PVOH film scale-up activities.

plan for large-scale commercialization of polymer film dc bus capacitors. In FY 2003, we developed, in conjunction with TPL, a continuous process for fabricating 450-ft-long rolls of SNL PVOH sheets. We investigated several different aspects of capacitor fabrication, including lower-temperature cures and adjustment of deposition parameters at Steiner Corporation to minimize the brittleness of SNL PVOH films. There are different termination procedures for wound polymer film capacitors. SNL polymer film wound capacitors of 1-µF capacitance were fabricated using two different termination techniques, metallized paper and high-volume electrodes, and with and without oil backfilling. These capacitors met the extended temperature requirements for fuel cell vehicles. In addition, we are supplying—on a continuous basis—dielectric films to Andrew Wereszczak of ORNL from our scale-up and development activities. Understanding mechanical property–process relationships is critical to developing film technology that exhibits adequate release from the underlying carrier. In FY 2004, we will concentrate our efforts on fabricating capacitors using aluminum foil rather than high-volume metallization processing. SNL PVOH film rolls fabricated at Brady Corporation will be used to fabricate a series of 1-µF and larger capacitors for evaluation by SNL, ORNL, GM, Ford, and Daimler Chrysler.

Presentations and Publications

1. D. Wheeler and G. Jamison, "Novel Polymer Film Synthesis Routes of Voltage and Temperature Stable Dielectrics," October 5, 1999.

2. B. A. Tuttle, D. Wheeler, G. Jamison and D. Dimos, "dc Buss Capacitors for PNGV Power Electronics," *Automotive Propulsion Materials 2002 Annual Progress Report*, U.S. Department of Energy, pp. 27–32, October, 2002.

3. B. Tuttle, J. Wheeler, G. Jamison, D. Williams, D. Wheeler, J. Cesarano and P. G. Clem, "Dielectric Materials for Fuel Cell Vehicles and Pulsed Discharge Applications," presented at the Dielectric Materials and Components for Pulsed Power Applications Workshop, Arlington, Virginia, June 2–3, 2003 (invited), to be published in the proceedings.

F. Mechanical Reliability of Electronic Materials and Electronic Devices

A. A. Wereszczak, L. Riester, H. -T. Lin, and M. K. Ferber
Ceramic Science and Technology Group
Oak Ridge National Laboratory
P.O. Box 2008, MS 6068, BLDG 4515
Oak Ridge, TN 37831-6068
(865) 576-1169; fax: (865) 574-6098; e-mail: wereszczakaa@ornl.gov

DOE Technology Development Manager: Nancy Garland
(202) 586-5673; fax: (202) 586-9811; e-mail: nancy.garland@ee.doe.gov
ORNL Technical Advisor: David Stinton
(865) 574-4556; fax: (865) 241-0411; e-mail: stintondp@ornl.gov

Contractor: Oak Ridge National Laboratory, Oak Ridge, Tennessee
Prime Contract No.: DE-AC05-00OR22725

Objectives

- Identify and use mechanical test methods that accommodate the testing of hydroxylated polystyrene (PVOH) dielectric film specimens (and geometries thereof) provided by Sandia National Laboratories (SNL).
- Measure and interpret mechanical properties of PVOH films and identify which are the best candidates for future manufacturing scale-up based on mechanical robustness.

Approach

- Perform mechanical properties microprobing on a suite of PVOH-elastomer films to quantify the elastic modulus (E) and hardness (H) of each.
- Perform additional mechanical tests (e.g., scratch-testing, indentation creep) in an effort to further assess the PVOH-elastomer films' propensity to crack or tear under a tensile strain.

Accomplishments

- Measured the E and H of 15+ PVOH-elastomer films, finding that the use of 4010 elastomer in PVOH resulted in lower E and H than the use of 5015 and tetraethylene glycol divinyl ether (TEGDE) elastomers in PVOH.
- Conducted scratch testing (which exploits a film's propensity to crack or spall) that showed PVOH-4010 films tend to be more spall resistant than PVOH-5015 and PVOH-TEGDE films.

Future Direction

- Measure the tensile strength distribution of the two down-selected elastomer-PVOH dielectric films as a function of temperature and link the strengths to the population of strength-limiting flaws.
- Predict and verify allowable manufacturing and service strains of elastomer-PVOH dielectric films.

Introduction

A primary focus of the Power Electronics effort in the Automotive Propulsion Materials Program is to develop polymer capacitor technology that will replace current electrolytic, dc bus capacitors for power electronic modules in hybrid electric vehicles. The ultimate objective is to make the power modules more compact while maintaining tight voltage and temperature requirements and long service life without compromise caused by mechanical breakdown of the dielectric film. Toward that end, we collaborated with SNL in this project to mechanically evaluate a suite of SNL-manufactured PVOH dielectric polymers that have the potential to satisfy the objectives. The present effort has two objectives: (1) measure baseline mechanical properties of that suite of PVOH compositions and interpret their results so as to suggest which are most suitable for manufacturing scale-up, and (2) quantify the mechanical performance of those manufactured films so manufacturers and end-users of these dielectric films may use them without mechanical breakdown.

Results

A suite of PVOH-elastomer films were provided by SNL for mechanical characterization. The PVOH films were fabricated so that each one used one of three different elastomers designated as 4010, 5015, and TEGDE in varied additive contents of up to 30 wt %. The PVOH-elastomer matrix is shown in Table 1. The films were spin-coated onto metallized (aluminum) silicon wafers; a representative cross-section of this three-material system is shown in Figure 1. The PVOH-elastomer film was nominally 600 nm thick and was well bonded to the aluminum metallization layer under it. Because of the small film thickness and strong bonding (i.e., film removal was prohibited), the mechanical characterization was limited to use of a mechanical property microprobe (MPM) and other techniques that could test the mechanical robustness of the PVOH-elastomer film in situ.

Table 1. Test matrix of elastic modulus and hardness tests

Dielectric film	Elastomer content	Anneal (°C)
PVOH	0%	220 and 250
PVOH/4010	5%	220 and 250
	15%	220 and 250
	20%	220 and 250
	30%	220 and 250
PVOH/5015	5%	250
	15%	250
	20%	250
	30%	250
PVOH/TEGDE	5%	250
	15%	250
	20%	250
	30%	250

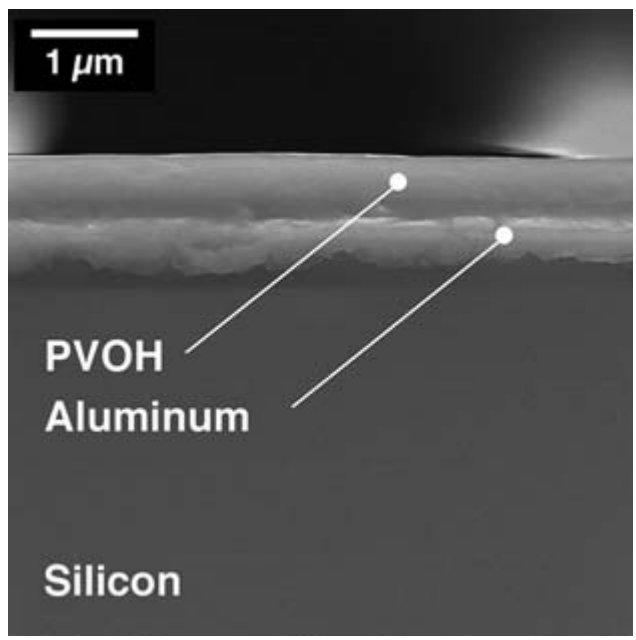

Figure 1. Cross-section of PVOH dielectric film (top), aluminum electrode layer (middle), and silicon substrate (bottom).

The MPM is an automated instrument consisting of four primary components: an indenter (Berkovich indenter) whose vertical displacement (nanometer resolution) and applied load (microgram resolution) are controllable; an optical microscope (OM)

with several objective lenses; a precision X and Y stage that translates the metallographically prepared specimen between the OM and the indenter; and a computer that controls the OM's lens turret (50–1500× magnification), stage movement, and indenter load and displacement. A schematic of the MPM is shown in Figure 2.

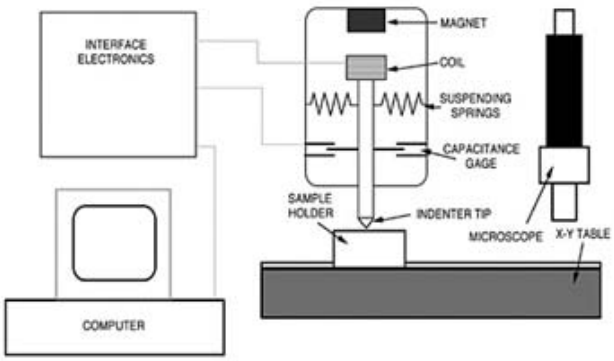

Figure 2. Schematic representation of the mechanical properties microprobe.

The computer also collects data on the indenter's displacement and load and is interfaced with a TV monitor and camera that show the microscope's field of view and allow inspection of each indentation. The MPM is housed inside an insulated cabinet that serves to minimize its susceptibility to laboratory room temperature fluctuations and vibrations (which are problematic when controlling displacement at the nanometer level). In a further effort to minimize the effects of vibration and thermal fluctuations, both the computer and the MPM-containing cabinet are housed in an insulated room within the laboratory.

The load/displacement history generated during indentation can be interpreted with the aid of an appropriate model to calculate the *E* and *H* of the material, as shown in Figure 3. *H* is calculated by dividing the peak load by the residual indent area, while *E* is determined from the slope of the unloading curve.

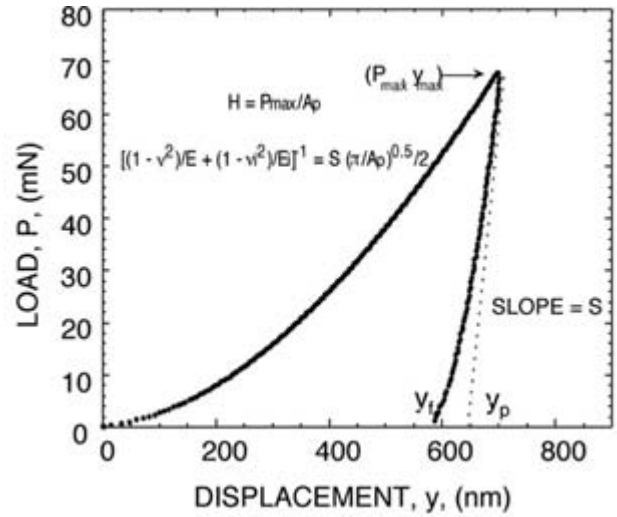

Figure 3. Typical load-displacement curve generated during and unloading with mechanical properties microprobe.

The measured *E* and *H* as a function of elastomer and elastomer concentration are shown in Figures 4 and 5, respectively. Sublayers under the top film can influence the apparent *E* and *H* of thin films if the indentation penetrates too far, so only *E* and *H* measurements from sufficiently shallow indentation depths (< ~10% of the PVOH film thickness) were considered. The *E* and *H* of the PVOH/4010 films tended to be of lower value than those of PVOH/5015 and PVOH/TEGDE films for a given additive content, particularly for additive content of 5 and 15%. The *E* and *H* of PVOH/4010, PVOH/5015, and PVOH/TEGDE were arguably equivalent for 20 and 30% additive content. Regarding the effect of annealing temperature on PVOH/4010, it was observed that annealing at 250°C rather than 220°C tended to increase the *E*, though *H* was essentially unaffected by the warmer temperature.

In an additional effort to distinguish differences among the PVOH films, indentation creep tests were performed on selected compositions (0%, 15% and 30% of each elastomer—all 250°C annealed) of the test matrix shown in Figure 1. A 5-mN load was applied, and the displacement of the deepening indenter penetration was

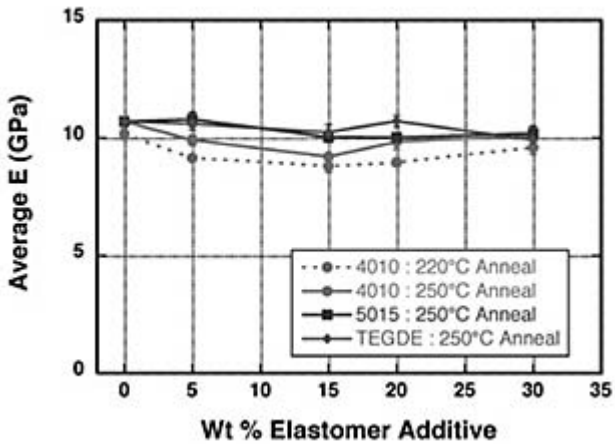

Figure 4. Comparison of elastic modulus as a function of elastomer additive content.

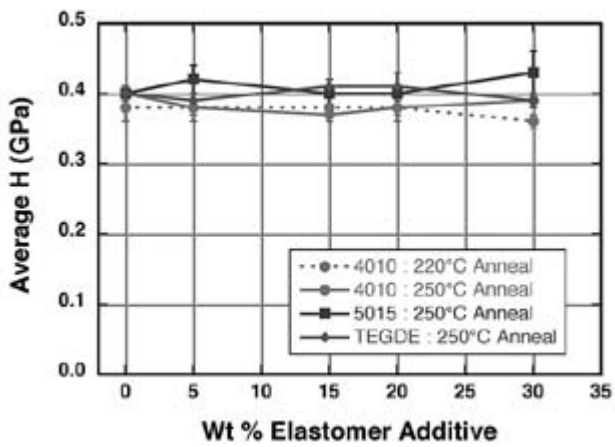

Figure 5. Comparison of hardness as a function of elastomer additive content.

measured as a function of time to 10 minutes. These results were found not to be a discriminator, as the measured creep responses of these seven films were equivalent, although the PVOH/30% TEGDE showed anomolously rapid creep deformation.

A limitation of the described indentation testing is that the results are all a consequence of compressive loading, whereas past observed cracking or tearing in PVOH (and other) dielectric films fabricated at SNL was a consequence of tensile straining. Even though that limitation was recognized early, prior to the indentation, the indentation proceeded because of the nature of the supplied PVOH/aluminum/silicon test coupons and because a tensile test could not be performed on that PVOH film. If differences in *E* or *H* or creep resistance among the PVOH films in the test matrix existed, then these compression-based mechanical tests would have found them, and those differences potentially could have been used to infer tensile performance. As described, though, the differences in *E* or *H* or creep resistances were nonexistent or subtle.

A series of scratch tests was performed on seven PVOH films (0% additive content and 15% and 30% content of 4010, 5015, and TEGDE) using a diamond stylus, and differences were analyzed. The use of such a test was pursued because it subjected a component of tensile strain to the PVOH film, and the performance of the film under a positive sign of strain could be examined. OM images in Figures 6–8 of the 0%, 15%, and 30% content 5015, respectively, show the former two PVOH films exhibited little or no spallation (i.e., brittleness), whereas there was significant spalling in the 30% 5015/PVOH film. Assuming that the material state of the films has not changed since the time of their deposition, the scratch test results suggest that the 4010/PVOH systems

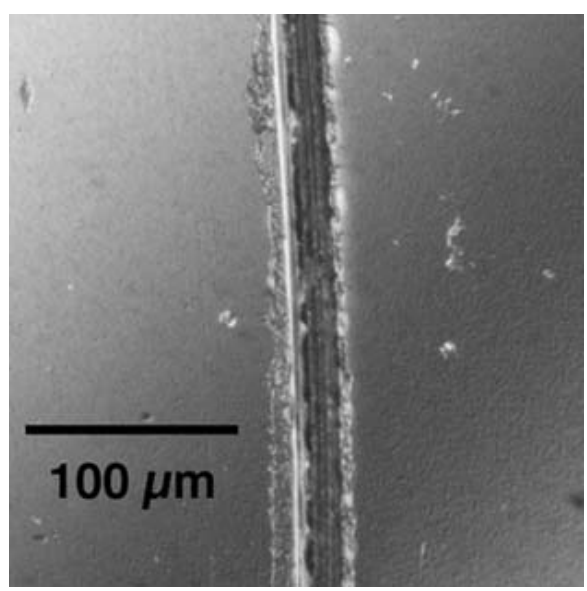

Figure 6. Scratch of PVOH (no elastomer).

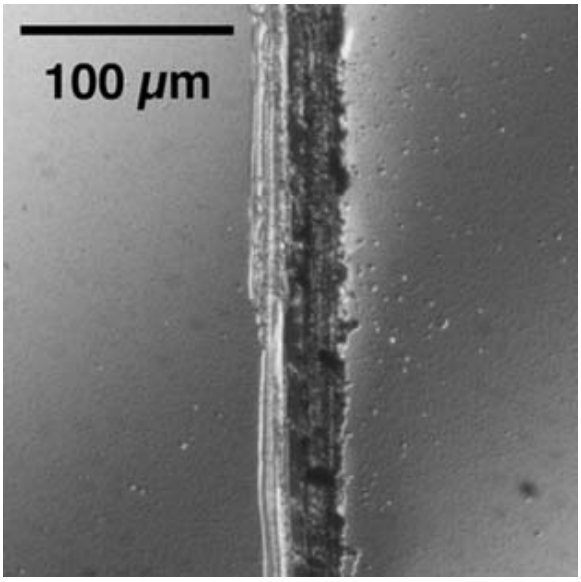

Figure 7. Scratch of PVOH 15% 5015/PVOH.

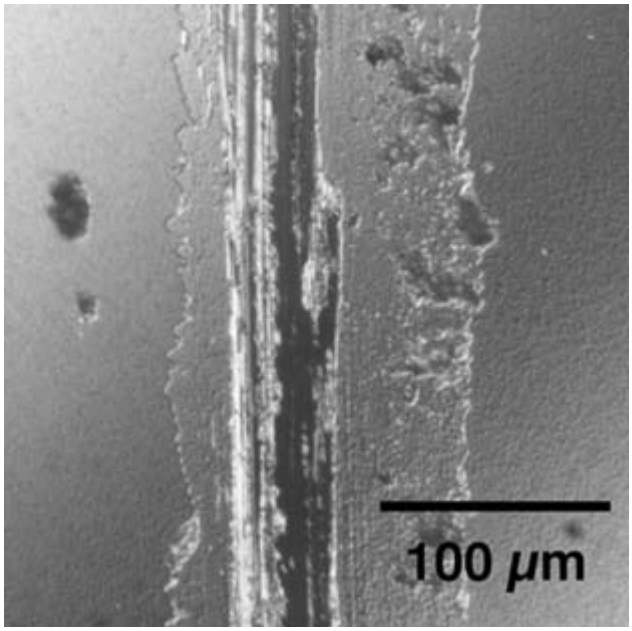

Figure 8. Scratch of 30% 5015/PVOH.

are the least brittle in that there was no significant evidence of spallation in the vicinity of the applied scratch for either the 15 or 30% concentrations of 4010. The 30% 5015 and 30% TEGDE films showed significant amounts of spallation around the scratch, indicating a greater degree of brittleness in those films. There was a small extent of lobing around the scratch in the 15% TEGDE film, indicating a moderate level of brittleness was being exposed.

Conclusions

Spallation is believed to be an indicator of brittleness, and this brittleness is likely linked to a PVOH dielectric film's propensity to tear or crack when strained in tension during manufacture or, ultimately, during service. The 0% PVOH, 15% 4010/PVOH, 15% 5015/PVOH, and 30% 4010/PVOH films exhibited little or no brittleness and are therefore the best candidates for manufacturing scale-up. This lack of brittleness in the PVOH containing the 4010 elastomer is perhaps consistent with its generally having lower *E* and *H* than the PVOH films that contain 5015 or TEGDE elastomers. If any of the examined films are apt to tear or crack when subjected to tensile straining, then those would be the 30% 5015/PVOH and 30% TEGDE/PVOH films.

3. CIDI ENGINES

A. Microwave-Regenerated Diesel Particulate Filter Durability Testing

Dick Nixdorf
Industrial Ceramic Solutions, LLC
1010 Commerce Park Drive, Suite I
Oak Ridge, TN 37830
(865) 482-7552; fax: (865) 482-7505; e-mail: nixdorfr@indceramicsolns.com

DOE Technology Development Managers: Rogelio Sullivan
(202) 586-8042; fax: (202) 586-1600; e-mail: rogelio.sullivan@ee.doe.gov

ORNL Technical Advisor: David Stinton
(865) 574-4556; fax: (865) 241-0411; e-mail: stintondp@ornl.gov

---

Contractor: Industrial Ceramic Solutions, Oak Ridge, Tennessee
Prime Contract No.: 4000000723
Subcontractors: Transportation Research Center, East Liberty, Ohio; Lydall Technical Papers, Rochester, N.H.

Objectives

- Develop, fabricate, and road-test a pleated ceramic fiber filter system that operates with reduced engine backpressure compared with conventional particulate filters, and investigate microwave regeneration at all engine operating conditions.
- Develop a microwave regeneration system that will operate at all engine load conditions.
- Conduct a road test of the pleated filter on the Ford F-250 diesel truck to test filter durability at high exhaust flow rates.

Approach

- Conduct air-flow and strength testing to establish an acceptable prototype pleated filter cartridge.
- Validate the filter system's particulate removal efficiency on a stationary diesel engine test cell.
- Install and road-test the improved microwave filter system on a 7.3-L diesel vehicle to verify durability.

Accomplishments

- Developed a pleated ceramic fiber filter cartridge and demonstrated that it achieved 1/10 the exhaust backpressure of a conventional wall-flow particulate filter while withstanding the forces of the truck exhaust.
- Completed efficiency testing on Oak Ridge National Laboratory's (ORNL's) 1.7-L Mercedes test cell to show greater than 96% removal of diesel particulate matter (PM) down to 10 nanometers.

- Designed, fabricated, and road-tested a pleated filter cartridge system and investigated microwave regeneration at engine idle condition on a 7.3-L Ford F-250 truck.
- Conducted the road testing of the pleated filter cartridges on the Ford F-250 diesel truck at a full range of engine operating conditions.

Future Direction

- Enlist exhaust system, catalyst, engine, and vehicle manufacturers in a joint product development effort to move toward commercialization of the ceramic fiber pleated particulate filter in 2004.
- Convert the rectangular pleated filter geometry to a round filter shape desired by the diesel industry to meet Environmental Protection Agency (EPA) 2007 Tier II requirements.
- Continue on-road testing on the 7.3-L Ford truck with the round pleated filter for an additional 10,000 miles, under high-load conditions, to extend the durability performance database.
- Partner with a volume filter cartridge manufacturer to provide large quantities of the pleated filter cartridges necessary to the diesel industry over the next 10 years.

Introduction

As diesel engine manufacturers and diesel vehicle original equipment manufacturers (OEMs) move closer to the 2007 EPA deadline for effective emission controls, the industry's requirements for the microwave-regenerated diesel PM filter system have become more defined. The alternative catalyst-regenerated systems, which require high exhaust temperatures, seem to be working reasonably well on heavy-duty diesel trucks (>10 L engine sizes). These engines account for about 25% of the diesel engine market in the United States. However, medium-duty trucks, buses, delivery vans, pickup trucks, and future diesel sport utility vehicles (SUVs) and off-road vehicles will need a self-heating particulate filter to operate under all conditions. This creates an opportunity in 75% of the diesel engine market for a demonstrated microwave-regenerated diesel particulate filter (DPF). There are number of actively heated DPFs under development, but none that have a proven record on an operating diesel vehicle. Industrial Ceramic Solution's (ICS's) completion of the FY 2003 DOE Propulsion Materials Program vehicle road test will place the microwave-regenerated DPF high on the list of viable active DPF systems.

In the FY 2003 work, a second product to control diesel particulates across all market applications has emerged—the ceramic fiber pleated filter cartridge itself. All of the approaches to PM control must use some form of a ceramic filter. To date, that filter has been an extruded honeycomb "wall-flow" product. Experiments conducted by ICS and others under the FY 2003 program have demonstrated that the pleated ceramic fiber DPF places much less exhaust backpressure on the diesel engine than do the wall-flow filters. This will improve engine performance and reduce the fuel penalty imposed by the PM control device. The pleated ceramic fiber DPF, which weighs significantly less than the extruded wall-flow filter, exhibits a lower thermal mass to achieve faster soot combustion temperatures and adds less weight to the vehicle. ICS is in discussions with many diesel engine and exhaust system manufacturers to test the pleated ceramic fiber filter cartridge in their existing regeneration technologies.

Approach

The first phase of the FY 2003 work was the development of the pleated ceramic fiber filter cartridge. Many experiments were conducted to determine the optimum

geometry of the filter and the best means to fabricate this geometry in the laboratory. A pleating process, using a ceramic binder, was developed. A number of structural designs to enclose and support the pleated fiber media in the exhaust were investigated. The finished product is shown in Figure 1. This cartridge was tested for exhaust backpressure properties against a wall-flow filter. Those data are presented in Figure 2. Since the pleated cartridge is a significant change from the wall-flow design the ICS has used for the last several years, verification of the PM removal efficiency was needed. Therefore, pleated filter cartridges were canned and tested by Oak Ridge National Laboratory

Figure 1. The new design of the ceramic fiber pleated filter cartridge.

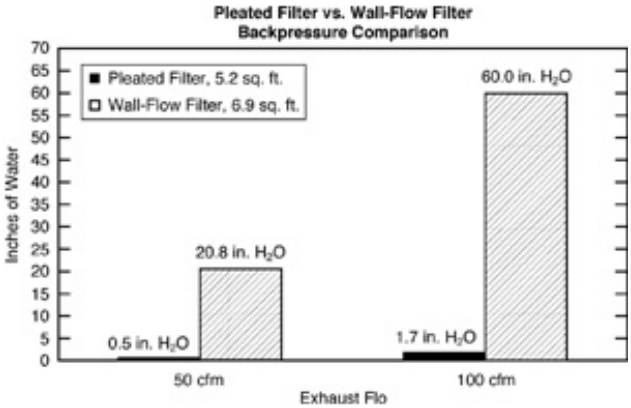

Figure 2. Exhaust backpressure comparison between the ICS pleated filter and a wall-flow filter.

(ORNL) on a 1.7-L Mercedes stationary test cell. The particulate removal efficiency from those tests is shown in Figure 3 for carbon mass and Figure 4 for diesel soot particle size distribution.

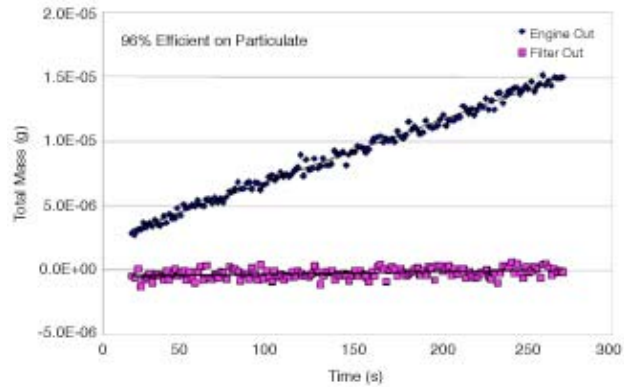

Figure 3. ORNL 1.7-L Mercedes test cell measurement of PM removal efficiency of the pleated filter.

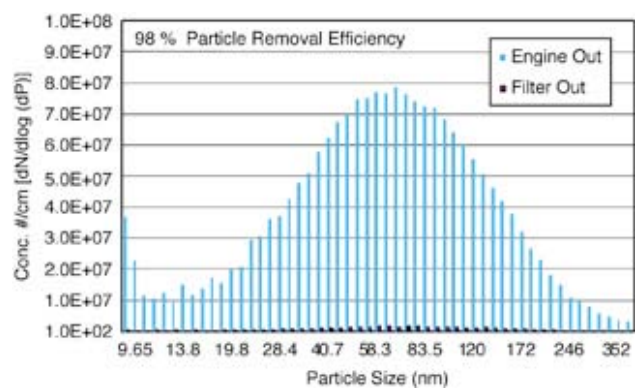

Figure 4. ORNL 1.7-L Mercedes test cell measurement of particle size distribution before and after the pleated filter.

The Oak Ridge testing, although highly successful in PM removal efficiency, showed a weakness in the filter cartridge strength; there were several ruptures in the filter media at high engine loadings. These results prompted ICS to spend another 6 months strengthening the media and the filter structure design. These improvements were tested on the exhaust system of the 7.3-L Ford truck and showed a 10× improvement in filter media strength. No media failures

have been recorded with the improved filter cartridge on the truck exhaust tests.

The microwave-regenerated DPF system, which will regenerate under any engine load condition, was designed and fabricated for the Ford F-250 7.3-L diesel truck. The system was fabricated and installed on the truck (Figure 5). It was installed in the bed of the truck to accommodate the temperature and pressure sensors and the need to disassemble the can to examine the filter cartridges periodically. Installation of the system under the truck would have created an impossible hardship, since ICS does not have a hydraulic lift available for the truck. All microwave equipment, system controls, monitoring sensors and computer data acquisition are installed on the truck for the road and track testing. As testing on the truck began, a noticeable deficiency in microwave heating of the cartridges was observed. Further investigation revealed that ICS had received a defective lot of silicon carbide fibers from the fiber manufacturer. Upon review of the fiber manufacturer's procedures, it was learned that a key processing parameter had been changed to achieve a higher product yield. This parameter was corrected, and a quality control procedure was implemented to prevent future occurrences of this problem. A proper lot of silicon carbide fibers were obtained. Converting these fibers to paper media, pleating the media, and fabricating it into filter cartridges delayed the truck testing by 6 months. All of the new cartridges have been fabricated, which will allow the track testing of the truck to begin in August 2003.

Figure 5. Microwave-regenerated pleated cartridge DPF installed on a Ford 7.3-L truck for testing.

Results

The pleated fiber filter cartridge offers several advantages over the conventional extruded ceramic wall-flow filter. The exhaust backpressure on the engine created by the DPF is decreased by a factor of 10 to 20 (Figure 2). The weight of the pleated cartridge will be approximately half that of the cordierite wall-flow product and one-third that of the silicon carbide wall-flow product. The PM removal efficiency of the pleated filter cartridge is 96% to 98% (Figures 3 and 4), which equals that of the conventional DPF products.

The microwave-regeneration system was tested on the Ford F-250 7.3-L diesel truck under high-idle exhaust flow conditions. Regeneration temperatures were not achieved because of a non-uniform microwave field. Road testing of the pleated filter on the 7.3-L diesel truck under a full range of engine operating conditions showed good durability and high potential for the use of the pleated DPF in commercial applications.

Conclusions

The pleated ceramic fiber filter cartridge has demonstrated lower backpressure and thermal mass properties that can make it a valuable addition to all types of PM regeneration systems. ICS is negotiating with

a major international filter manufacturer to license the use of the technology to supply the large volumes of filter cartridges that will be necessary to supply the worldwide diesel industry. Completion of the successful road testing of the Ford diesel truck will allow ICS to demonstrate the truck to several U.S. diesel engine and vehicle OEM suppliers. This exercise will convince one or more of these companies to investigate the incorporation of the round, pleated ceramic fiber filter in their total emissions control solution for light-duty vehicles. Support by diesel engine manufacturers and vehicle OEMs is expected to lead to fleet testing and eventual commercial use. The pleated ceramic filter cartridge DPF can solve many problems that exist for companies seeking particulate control solutions for 2007 and beyond.

FY 2003 Publications/Presentations

"Microwave-Regenerated Particulate Filter," presented at the DOE National Laboratory Advanced Combustion Engine R&D Merit Review and Peer Evaluation, Argonne National Laboratory, May 13–15, 2003

B. Material Support for Nonthermal Plasma Diesel Engine Exhaust Emission Control

Stephen D. Nunn
Materials Processing Group
Oak Ridge National Laboratory, P.O. Box 2008, MS 6087
Oak Ridge, TN 37831
(865) 576-1668; fax: (865) 574-4357; e-mail: nunnsd@ornl.gov

DOE Program Manager: Rogelio Sullivan
(202) 586-8042; fax: (202) 586-1600; e-mail: rogelio.sullivan@ee.doe.gov

ORNL Technical Advisor: David Stinton
(865) 574-4556; fax: (865) 574-6918; e-mail: stintondp@ornl.gov

---

Contractor: Oak Ridge National Laboratory, Oak Ridge, Tennessee
Prime Contract No.: DE-AC05-00OR22725

Objectives

- Identify appropriate ceramic materials, develop processing methods, and fabricate complex-shaped ceramic components that will be used in nonthermal plasma (NTP) reactors designed by Pacific Northwest National Laboratory (PNNL) for the treatment of diesel exhaust gases.
- Fabricate and ship components to PNNL for testing and evaluation in prototype NTP reactors.
- Develop a component design and establish a fabrication procedure that can be transitioned to a commercial supplier.
- Assemble a prototype NTP reactor and test it on a laboratory diesel engine.

Approach

- Evaluate commercially viable forming methods to fabricate complex-shaped ceramic components that meet PNNL design specifications.
- Modify processing as needed to accommodate material and design changes.
- Evaluate bonding and sealing materials for preparing assemblies of the ceramic components.
- Fabricate components and assemblies for testing and evaluation.

Accomplishments

- Fabricated more than 16 ceramic dielectric plates for assembly of full stacks (7 individual plates) to be used in the NTP reactor.
- Conducted shear strength experiments to determine the strength of the sealing glass bond between joined ceramic components.
- Fabricated a full-scale stainless steel sheet metal housing for the NTP reactor assembly.

Future Direction

- Complete the evaluation of sealing materials to bond and seal the various ceramic and metal components of the NTP reactor into a complete assembly for functional testing.
- In collaboration with PNNL, finalize the NTP reactor design for assembly and testing to determine the durability and operational performance of the device.
- Fabricate an NTP reactor assembly and conduct tests of the device on a 1.7-L diesel engine.

Introduction

NTP reactors have been shown to be effective devices for reducing unwanted nitrogen oxides and particulate exhaust gas emissions from diesel engines. Researchers at PNNL are developing new, proprietary design configurations for NTP reactors that build on past experimental work. To improve effectiveness, these designs include ceramic dielectric components having complex configurations. Oak Ridge National Laboratory (ORNL) has extensive experience in the fabrication of complex ceramic shapes, primarily based on prior work related to developing ceramic components for gas turbine engines. The ORNL expertise is being utilized to support PNNL in its development of the new NTP reactor designs.

Approach

Collaborative discussions between ORNL and PNNL are used to establish new ceramic component designs for improved NTP reactors. Meeting NTP reactor design objectives is balanced with the limitations of ceramic manufacturability to arrive at a new component configuration. The ceramic processing facilities and expertise at ORNL are then used to establish fabrication capabilities and to produce components for testing at PNNL. This is an iterative process as both parties gain more knowledge about fabricating the components and about their performance in NTP reactor tests. The ultimate goal is to identify a design that performs well and that can be readily produced by a commercially viable process.

Results

A supply of ceramic dielectric plates was fabricated from Dupont 951AX Green Tape®. This tape-cast ceramic material can be formed and bonded together as described in previous reports. Figure 1 shows examples of

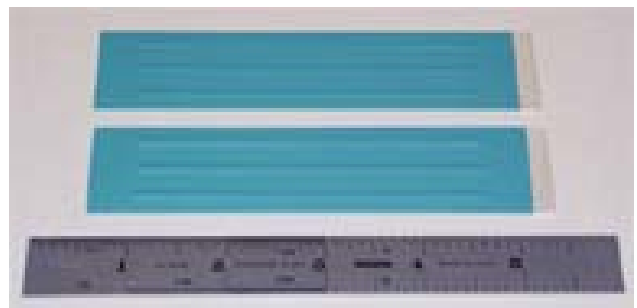

Figure 1. Individual ceramic dielectric plates fabricated from Dupont 951AX Green Tape®.

the ceramic plates. The ridges on the plates are hollow, and the interior surface of each ridge is coated with a silver electrode that extends to the outer surface at one end of the plate. When the plates are stacked and a strong electric field applied, there is a field concentration along the opposing ridges of the plates that initiates a plasma discharge. In constructing the NTP reactor that is being planned for testing on a small diesel engine, a stack assembly of seven individual plates will be used (Figure 2). The plates are separated by ceramic spacers that define the exact spacing between the opposing ridges. Sealing glass is used to join the spacers and the plates and to provide a gas-tight seal.

A test fixture was designed and fabricated to measure the shear strength of bonded samples of the ceramics used in the NTP

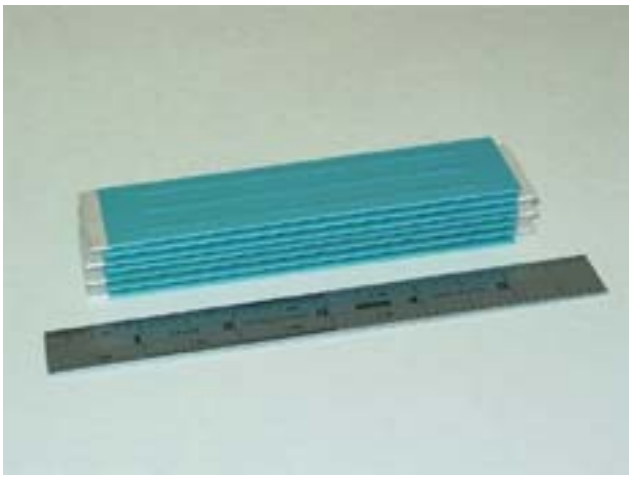

Figure 2. Example of a 7-layer ceramic dielectric plate stack that will be used in the experimental NTP reactor.

reactor assembly. This fixture is shown in Figure 3, along with one of the test samples. Using standard testing procedures, the bond strength achieved using different sealing glass compositions was evaluated and compared. Each test sample consisted of a ceramic button bonded to a small ceramic plate with the sealing glass. Test specimens of the ceramic were bonded together and placed in the test fixture, and an increasing shear load was applied until failure occurred. Examples of two test samples that underwent the shear strength test are shown in Figure 4. The two principal sealing glass candidates are lead-free glass compositions manufactured by Ferro Corporation, designated as EG2964 and EG2998. Figure 5 shows a comparison of the shear strength of these two materials. The results of the tests will be used along with other factors, such as thermal cycling stability, to select the best sealing glass composition for making the NTP assemblies. In preparation for testing the NTP reactor on a laboratory diesel engine, a full-size model of the NTP housing has been made. The housing will hold the ceramic dielectric plate stack in position and connect to the engine exhaust system. Figure 6 shows the housing, along with the ceramic dielectric stack it will contain. The model is being used to check the fit of the dielectric stack and the

Figure 3. Shear test fixture assembly used to measure the shear strength of the sealing glass joint.

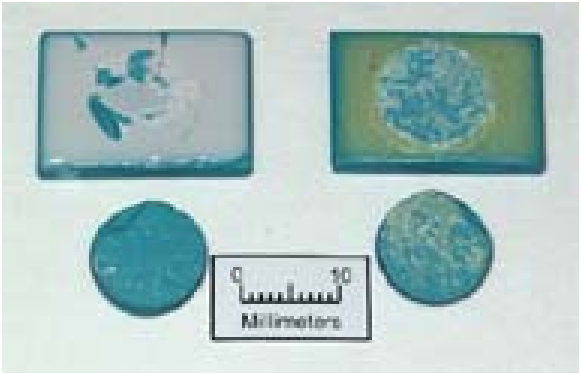

Figure 4. Shear test specimens of glass compositions EG2964 (left) and EG2998 (right) after testing.

assembly and sealing procedures so any necessary design changes can be incorporated before the final housing is fabricated from stainless steel sheet material. The engine tests, currently planned for a 1.7-L diesel engine, will evaluate the

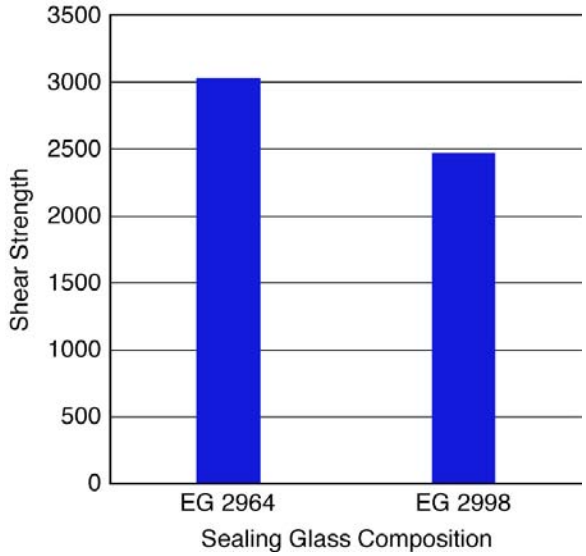

Figure 5. Results of the shear strength test measurements on glass compositions EG2964 and EG2998.

Figure 6. Stainless steel sheet metal NTP reactor housing and ceramic dielectric stack.

durability and function of the NTP assembly under engine operating conditions.

Conclusions

A supply of ceramic dielectric plates has been fabricated for the assembly of stacks to be used in an experimental NTP reactor that will be tested on a small diesel engine. A shear strength test apparatus was used to measure the bond strength of sealing glass compositions that are being evaluated for use in assembling the ceramic dielectric stacks. The two compositions under consideration, Ferro Corp. EG2964 and EG2998, had average shear strengths of 3034 psi and 2476 psi, respectively.

A prototype NTP reactor housing was fabricated from stainless steel sheet metal. Using the prototype, the final dimensions required to accommodate the dielectric stack and to attach it to the exhaust system of a 1.7-L laboratory diesel engine can be determined.

C. Fabrication of Small Fuel Injector Orifices

John B. Woodford, George R. Fenske
Argonne National Laboratory
9700 South Cass Avenue
Argonne, IL 60439
(630) 252-0910; fax (630) 252-4798; e-mail: gfenske@anl.gov

DOE Technology Development Manager: Rogelio Sullivan
(202) 586-8042; fax: (202) 586-1600; e-mail: rogelio.sullivan@ee.doe.gov

---

Contractor: Argonne National Laboratory, Argonne, Illinois
Prime Contract No.: W-31-109-Eng-38

Objectives

- Develop a methodology for reducing the diameter of fuel injector orifices to 50 µm by applying material to the internal diameter (ID) of the orifice.
- Characterize the spray and combustion properties of the fuel injector systems so treated.
- Transfer the technology to an industrial partner.

Approach

- Evaluate the potential of electroless nickel (EN) plating for reducing orifice diameter, identify the critical barriers to commercialization, and resolve those barriers.
- Evaluate the potential of EN plating for improving surface finish and reducing deposit formation on injector nozzles.

Accomplishments

- Successfully reduced the orifice diameter of diesel engine fuel injectors from 200 µm to 50 µm with EN plating.
- Compared the surface roughness of coatings deposited by EN plating at various thicknesses and under various conditions.
- Conducted initial testing that indicates that EN plating reduces by nearly twofold the mass of deposit formation on the injectors.
- Initiated contact with International Harvester/Navistar regarding possible transfer of the plating technology.

Future Direction

- Characterize the spray characteristics of coated injectors.
- Prepare coated injector tips for flame spray characterization tests.
- Perform further tests on deposit formation using alloy coatings.

Introduction

Recent work on the control of particulate matter (PM) emissions and improvement of engine combustion efficiency in diesel engines has shown the effectiveness of reducing the diameter of injector orifices in promoting fuel atomization, leading to more complete combustion and reduction in soot formation.[1,2] The current industry target is a 50-µm diameter; however, because mean droplet size and soot incandescence both decrease steadily with orifice diameter, any reduction in orifice diameter should result in improved efficiency and reduced PM emissions. Advancements in the electrodischarge machining (EDM) technology currently used to fabricate orifices are not expected to achieve the 50-µm target nor to alleviate the rough interiors produced by EDM. Currently, orifices produced by EDM must be polished using an abrasive slurry to achieve an acceptable surface finish of around 0.5 µm R_A with a surface morphology characterized by sharp peaks and valleys. During the fuel injection process, this morphology leads to a highly turbulent layer adjacent to the wall, which reduces the effective fuel delivery area of the orifice. As the orifice diameter is pushed down toward 50 µm, the impact of surface finish is greatly magnified, thus demanding an even smoother finish.

In addition to being a potential route to economical production of 50-µm diameter fuel injector orifices, EN plating offers potential solutions to the problems of soot formation and surface roughness. It is possible to deposit coatings with different surface chemistries, some of which may reduce the propensity of diesel fuel to form deposits on the injector nozzle. The morphology of EN-plated surfaces appears to be generally smoother, as well.

Approach

As documented in the 2002 annual report, EN plating was selected over a number of alternative coating processes because of its cost, maturity, and potential to coat interior surfaces. EN plating is a method of depositing nickel/phosphorus or nickel/boron alloys onto metallic surfaces from aqueous solution, although other metals may be deposited using the same principle. We plan to perform further evaluations of the suitability of EN plating for ID reduction in orifices, for mitigating deposit formation, and for changing the surface morphology of the underlying substrate material.

Results

As a result of interactions with Siemens' injector supplier, we began to consider surface roughness as a critical parameter. We performed a number of trials using different deposition methods to determine the change in surface roughness with EN plating at various thicknesses and under various deposition conditions. Figure 1 contains a plot of R_A values for orifice walls plated under different conditions, compared with the R_A value of an unplated orifice wall. As part of this study, we also established that although ultrasonic agitation of the plating bath increases the deposition rate, it also tends to increase the surface roughness compared with the unplated surface. In general, the longer the plating time, the smoother the plate.

Erosion due to cavitation is expected to be a major problem in fuel injectors as orifice diameter decreases and injection pressure increases. The mechanical properties of EN plating depend upon the amount of phosphorus in the plate, its microstructure, and its thermal history. In order to determine the effect of plating bath composition on the plate's mechanical properties, we measured the Knoop hardness of the plate as a function of position (and thus bath depletion) (Figure 2). The first plate to be deposited is hardest; then, as the bath depletes, the plate hardness decreases. Thus we should be able to tailor the plating

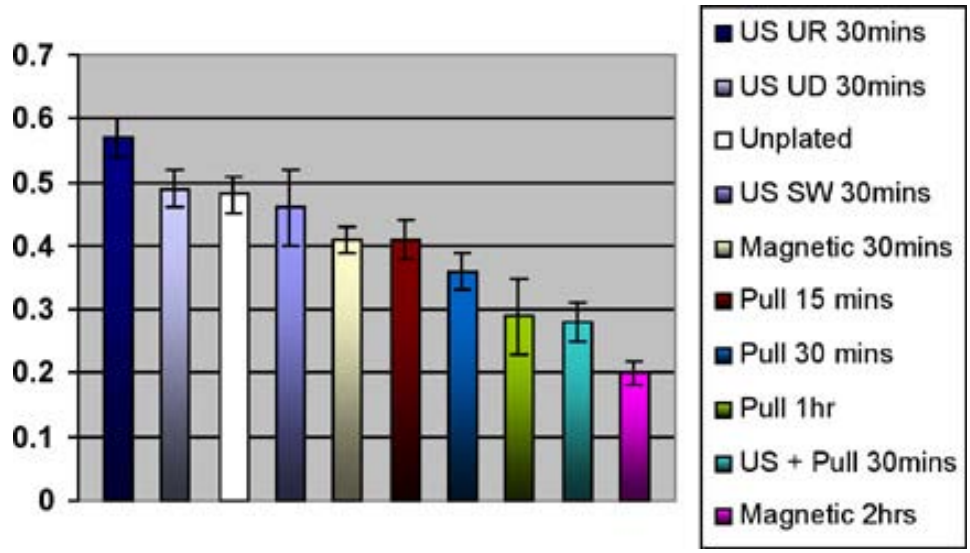

Figure 1. Surface roughness R_A for different deposition conditions.

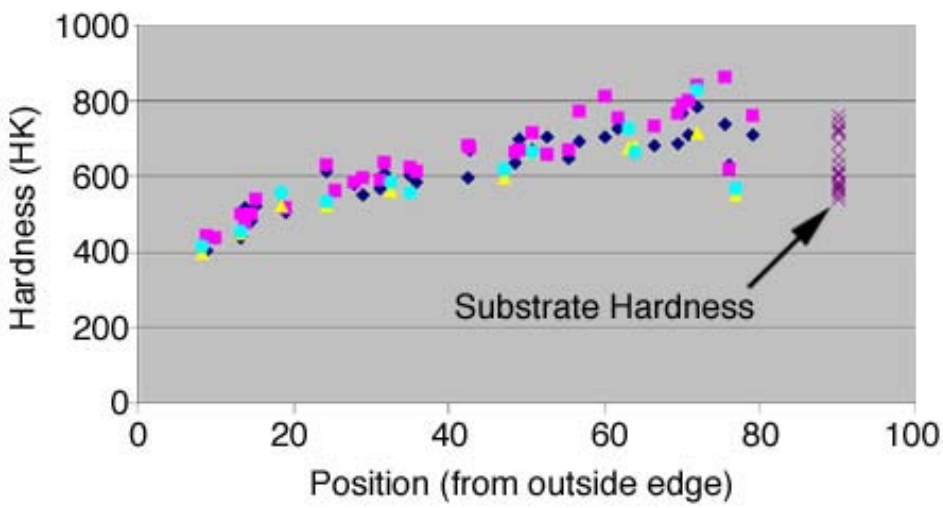

Figure 2. Knoop hardness of the nickel plate as a function of position.

hardness for maximum erosion resistance by maintaining the bath composition at a particular level.

We designed, constructed, and tested a system for forced-circulation plating of multiple injectors (Figure 3). To avoid the previous difficulty with orifice clogging, the bath is filtered before being pumped into a multiple-injector manifold. Initial test results showed that forcing circulation at even modest pressures resulted in marked reduction in deposition rate on the orifice interior (Figure 4). However, the coating on the orifice interior was also quite smooth. Further work is ongoing.

As described earlier, deposits are expected to be a significant problem for small orifices. Thus we have begun to characterize the relative vulnerability of EN-plated injectors to deposit formation. Initial tests involved heating plated and unplated injector surfaces to around 240ºC, dropping diesel fuel onto them, and measuring the change in mass. We expected the nickel plate to be less

Figure 3. Forced-circulation plating system.

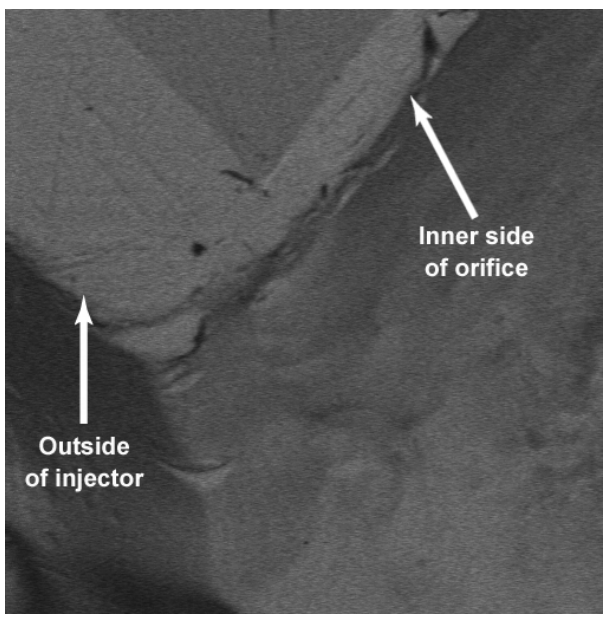

Figure 4. Micrograph of the outer edge of the plated orifice, showing the difference in thickness between the orifice interior and the injector exterior.

susceptible to deposit formation than pure nickel (also tested for comparison) as a result of the presence of phosphorus in the coating. Figure 5 shows the results. The EN plating affords a nearly twofold reduction in deposit mass over the unplated steel. We are planning further tests to characterize the deposits and their adhesion to the metal surface.

Before the large forced-circulation plating system was completed, we attempted another method of forcing bath circulation through the injector. Spinning the injector in the plating bath resulted in a low, constant flow of plating bath through the injector. Using that method, we have successfully reached and surpassed the ID goal of 50 μm (Figures 6 and 7).

Conclusions/Future Work

The work done in the past year has demonstrated the promise of EN plating as a technique for meeting the current industry target for fuel injector orifice diameter. We have also shown its potential for reducing plugging due to deposit formation and for improving the surface finish of the orifice interior.

Following the recommendations of a peer review panel, our future efforts will include further testing, including benchmarking the coated injectors vs uncoated injectors in terms of their surface hardness, discharge coefficient, spray form, hole-to-hole variation, and target accuracy. Following this evaluation, engine testing and/or commercial evaluation have been strongly encouraged. We have been advised to investigate the use of maskants and/or special fixturing to restrict plating to the nozzle area. Another reviewer pointed out that hole geometry is a critical design parameter and said that we should determine orifice circularity. These are all excellent suggestions, and we intend to work on all of them, on our own and in concert with Argonne National Laboratory–Energy Systems personnel. We will also solicit further assistance in testing from our industrial contacts.

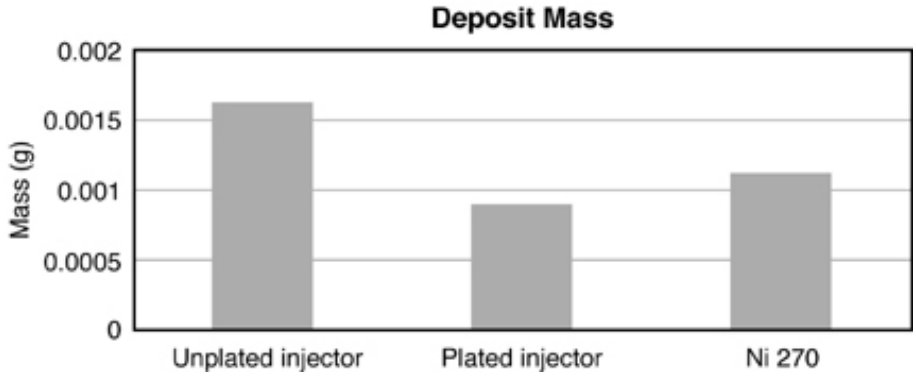

Figure 5. Deposit mass on pure nickel, unplated injector segment, and plated injector segment.

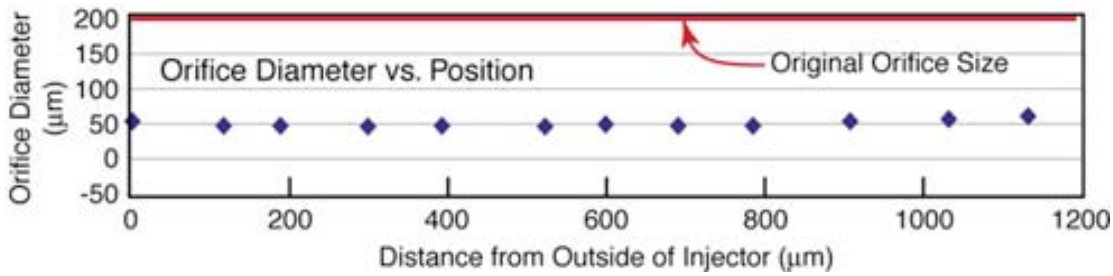

Figure 6. Plot of coating thickness as a function of position along the orifice.

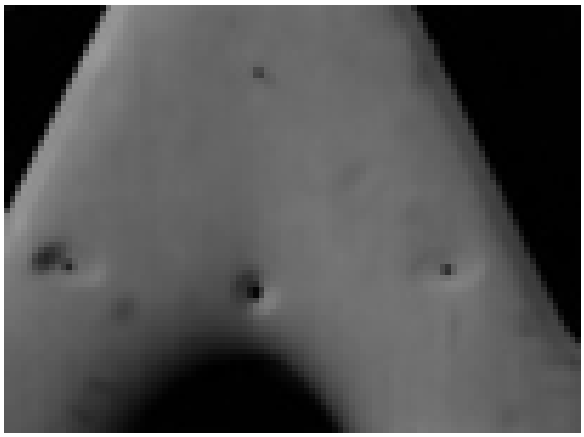

Figure 7. Micrograph, cross-section of coated injector tip.

References

1. John B. Heywood, *Internal Combustion Engine Fundamentals*, McGraw-Hill, 1988.

2. Lyle M. Pickett and Dennis L. Siebers, Paper No. 2001-ICE-399, Internal Combustion Engines-Vol. 37-1, *Proceedings of the 2001 Fall Technical Conference, American Society of Materials Engineers 2001*, Ed. V. W. Wong, American Society of Materials Engineers, 2001.

D. Technology for Producing Small Holes in Advanced Materials

Stephen D. Nunn
Materials Processing Group
Oak Ridge National Laboratory, P.O. Box 2008, MS 6087
Oak Ridge, TN 37831
(865) 576-1668; fax: (865) 574-4357; e-mail: nunnsd@ornl.gov

DOE Program Manager: Rogelio Sullivan
(202) 586-8042; fax: (202) 586-1600; e-mail: rogelio.sullivan@ee.doe.gov

ORNL Technical Advisor: David Stinton
(865) 574-4556; fax: (865) 574-6918; e-mail: stintondp@ornl.gov

---

Contractor: Oak Ridge National Laboratory, Oak Ridge, Tennessee
Prime Contract No.: DE-AC05-00OR22725

Objectives

- Explore methods for producing ultra-small holes (<50μm) in advanced materials for fuel injector nozzles.
- Evaluate carbide-based cermets and high-temperature ceramics as candidate materials.
- Devise methods to produce precisely a desired pattern of holes having a well-controlled size and shape.
- Investigate methods to fabricate fuel injector shapes or inserts having ultra-fine holes.

Approach

- Form holes in situ during the sintering process by incorporating various pore formers in the green (unsintered) body while it is being shaped.
- Use nickel alloy wires in nickel aluminide-bonded (Ni_3Al-bonded) titanium carbide (TiC) to form holes during sintering.
- Embed into gelcast ceramic materials combustible organic fibers that will vaporize during sintering at high temperatures.
- Gelcast ceramic materials around metal wires that can be removed from the green body prior to sintering, leaving a hole in the part.
- Evaluate thermalplastic coextrusion as a method to form a complex hole-forming pattern in ceramic materials.

Accomplishments

- Produced holes of 108, 76, 51, and 26 μm in diameter in a TiC-Ni_3Al cermet composition.
- Formed 8-hole arrays of ~50-μm-diam holes in gelcast alumina and zirconia ceramics.
- Formed fuel injector nozzle shapes containing an array of fine holes in alumina and zirconia ceramics by gelcasting in a plastic mold with metal wire inserts.
- Fabricated a 6-hole array of 30-μm-diam holes in alumina ceramic using thermalplastic coextrusion.

Future Direction

- Fabricate a precision mold to gelcast ceramic fuel injector nozzles.
- Evaluate joining methods for producing hybrid steel-/ceramic-tip fuel injector nozzles.
- Assess the durability of advanced ceramics in the diesel engine combustion environment.

Introduction

To meet the ever-growing demand for improved efficiency and reduced emissions, future fuel injection systems will require improvements in both design and materials. The objective of this project is to explore new methods for forming ultra-small (<50-µm) holes in advanced materials. Carbide-based cermets (ceramic/metallic composites) and high-temperature ceramics are candidate materials to be used in this study. They have the desirable properties of high strength, high modulus, and low density compared with steel. In addition, they are corrosion resistant and, because of their high hardness, are resistant to wear and erosion.

Currently, fuel injector nozzle holes in steel are 150 to 200 µm in diameter. This size is at the limit for machined holes. One of the major challenges to using advanced materials for improved nozzles is the lack of capability to manufacture very fine holes in the densified material by conventional machining processes. To overcome this limitation, this project will explore methods for the in situ fabrication of holes during the sintering step that is a normal part of the fabrication process for advanced materials. Various techniques for incorporating fugitive pore-formers will be investigated. These pore-formers will be incorporated in the unsintered (green) body during the forming process and will be removed before or consumed during the sintering step to leave precisely-controlled pores (holes) in the densified material. If successful, this technique will not only allow the formation of simple holes but also add the potential to form holes having variable geometries.

Approach

It has been observed in past studies of the cermet Ni_3Al-bonded TiC that metal particles in the unsintered powder compact can leave voids in the sintered part because the metal is drawn into the carbide particle array by capillary action when the metal becomes molten. This tendency will be exploited in the present study to intentionally form holes in predetermined locations. Nickel alloy wires of the appropriate size will be located in the unfired material to form fine holes in the sintered part.

Two ceramic materials were selected for investigation in this project, alumina (Al_2O_3) and zirconia (ZrO_2). To form holes in the ceramics, fugitive pore formers will be incorporated in gelcast ceramic green bodies. Gelcasting is a method of forming powdered materials into complex shapes. Organic monomers are added to an aqueous slurry of the ceramic powder. When a polymerization reaction is initiated, the organic molecules and the slurry are transformed into a solid (gelled) body. By casting the slurry in a mold and then gelling it, a complex-shaped part can be formed. One approach to forming holes in the gelcast ceramic part is to place fibers in the mold that are trapped in desired locations in the gelled part. These fibers are burned away during the sintering process, leaving holes in the densified part. The fibers can be synthetic polymers (e.g., nylon, polyethylene), natural fibers (cotton, silk), or even graphite.

The second approach to forming holes in gelcast ceramic parts is to locate fine metal wires within the casting mold. Like the fibers, the metal wires are trapped in the gelled part. But rather than being burned

out, the wires can be withdrawn from the green body prior to sintering. Very fine holes that are formed in the green part can be retained in the sintered ceramic.

Another method being evaluated for forming holes in ceramic materials is the use of coextrusion to form complex arrays of holes on a very fine scale. The coextrusion process involves blending powder materials in a thermalplastic resin and then assembling segments of the filled resin to form a desired pattern. Each segment can contain a different filler material. In the present study, the segments contain either alumina ceramic or carbon powder, and the segments are arranged to form a hexagonal array of carbon-filled "holes" in an alumina matrix. The assembly is then extruded to reduce the cross-sectional area while retaining the segment pattern. The coextrusion can be repeated until the desired reduction of the segment pattern is achieved.

Results

A powder compact of Ni_3Al and TiC containing small lengths of nickel wire was prepared; several different diameters of nickel wire were incorporated in the specimen. At the firing temperature used to sinter the compact, the nickel became molten and was drawn into the surrounding powder matrix by capillary action, leaving a void where the wire had been. After sintering, the sample was sectioned, polished, and examined by optical microscopy. Elongated holes were observed in the otherwise dense body. The holes had measured diameters of 108, 76, 51, or 26 μm, depending upon the initial size of the nickel wire embedded in the sample. One of the holes in the cermet is shown in the scanning electron microscopy (SEM) micrograph in Figure 1.

Fine holes that were produced in a gelcast alumina ceramic sample by incorporating organic fibers were examined by SEM. An example is shown in Figure 2, where the hole is intersected at an oblique angle by the polished surface of the sample. The hole is approximately 30 μm in diameter. One interesting feature is that the surface roughness of the hole is at a scale defined by the grain boundary curvature of the individual crystallites that form the sintered ceramic. These crystallites average 2–3 μm in diameter. The curvature forms shallow grooves at the grain boundaries that are no more than 100 nm deep. This is an extremely fine surface finish that should minimize turbulence in fluid flowing in such a hole.

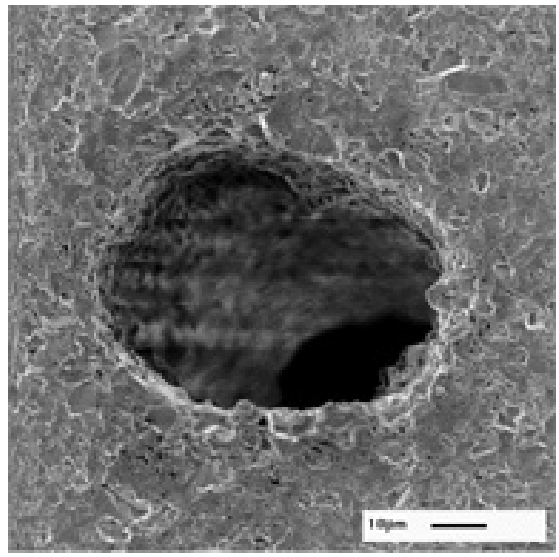

Figure 1. SEM micrograph of a 76-μm hole formed in an Ni_3Al–TiC cermet material.

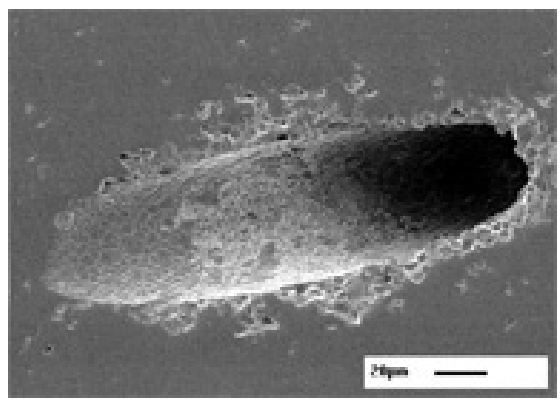

Figure 2. SEM micrograph showing the fine surface finish on a 30-μm hole formed by embedding an organic fiber in gelcast Al_2O_3.

A mold design was developed for gelcasting ceramic material in the shape of a fuel injector nozzle. The plastic mold was designed with removable wires in fixed locations to produce a controlled array of holes in the gelcast ceramic. An optical micrograph of the 8-hole array in the unfired part is shown in Figure 3. The sintered part is shown in Figure 4, along with a steel fuel injector nozzle that was used as the model for making the mold.

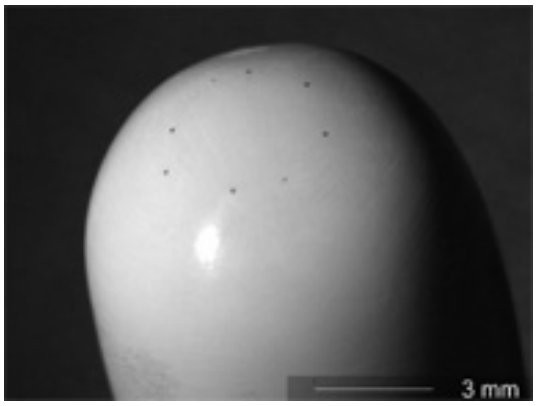

Figure 3. Optical micrograph of an 8-hole array formed on the tip of a fuel injector nozzle shape by incorporating removable metal wires in gelcast ZrO_2.

Figure 4. Gelcast and sintered ZrO_2 fuel injector nozzle shape (left) containing an array of eight holes in the tip. A steel nozzle is shown at right.

A coextrusion process was used to fabricate rods of unfired alumina ceramic containing a hexagonal array of fugitive hole-formers. Figure 5a shows two extruded rods approximately 50 mm long and 5 mm in diameter. The hole-forming array runs through the entire length of the rods. A thin disk was cut from the length of one of the rods; the optical micrograph in Figure 5b shows the cross-sectional view of the hole-forming array on the disk. Disks were fired at a high temperature to sinter the ceramic and burn away the fugitive material in the holes. After firing, the disks were about 4 mm in diameter as a result of sintering shrinkage, and the holes were about 32 μm in diameter. One of the holes is shown in the SEM micrograph in Figure 6. These disks could be used as inserts in a steel housing to form a hybrid fuel injector nozzle with ultrafine holes.

Conclusions

Fine holes of various sizes were produced in a Ni_3Al–TiC cermet material by incorporating fine nickel wires in the powder compact prior to sintering. Holes as fine as 26 μm in diameter were produced using this method.

SEM examination of holes produced in gelcast Al_2O_3 by trapping organic fibers in the casting and then burning them away during the sintering process revealed an exceptionally smooth surface finish on the holes that were formed.

A mold was designed to produce a controlled array of holes in gelcast ceramics having a fuel injector nozzle shape. A circular array of eight holes was formed in the tip of the nozzle shape.

Coextrusion was shown to be a viable forming method for producing an array of fine holes in Al_2O_3 ceramic.

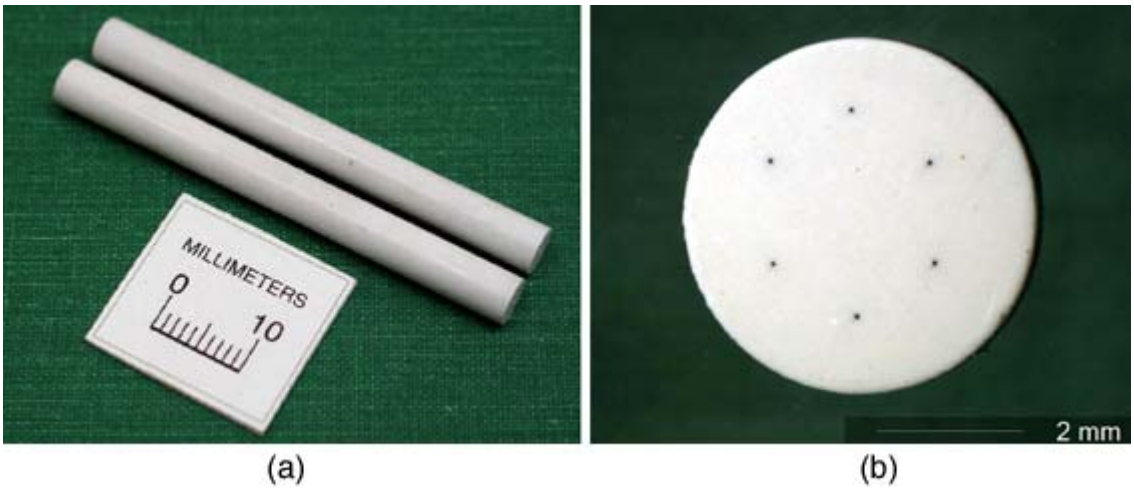

Figure 5. (a) Coextruded alumina rods 50 mm × 5 mm containing a hexagonal array of hole-formers. (b) Cross-section of a coextruded alumina rod showing the hole-forming array.

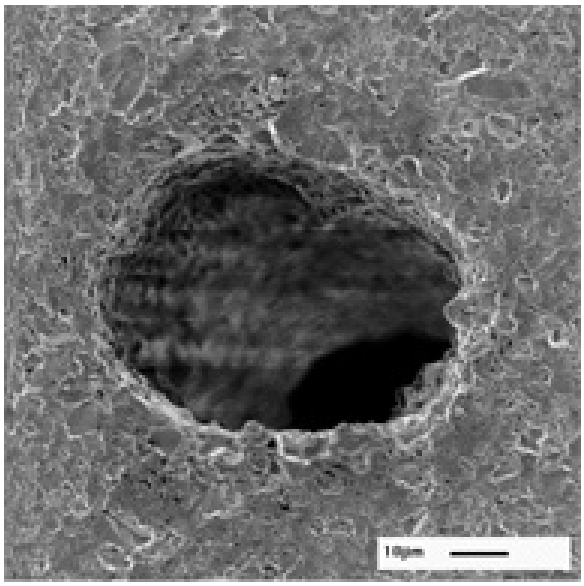

Figure 6. SEM micrograph of a hole in the coextruded alumina after sintering.

E. Electrochemical NO_x Sensor for Monitoring Diesel Emissions

L. Peter Martin and Robert S. Glass
Lawrence Livermore National Laboratory
P.O. Box 808, MS L-353
Livermore, CA 94551-0808
(925) 423-9831; fax: (925) 423-7040; e-mail: martin89@llnl.gov

DOE Program Manager: Rogelio Sullivan
(202) 586-8042; fax: (202) 586-1600; e-mail: rogelio.sullivan@ee.doe.gov

---

Contractor: Lawrence Livermore National Laboratory, Livermore, California
Prime Contract No.: W-7405-Eng-48

Objectives

- Develop a compact, rapid-response electrochemical nitrogen oxide (NO) or total nitrogen oxides (NO_x) sensor for compression-ignition, direct-injection (CIDI) exhaust gas monitoring.
- Demonstrate the commercialization potential of a new NO_x sensor technology developed during FY 2002.
- Collaborate with the Ford Research Center to optimize sensor materials, operating parameters, and performance.

Approach

- Use an ionic (O^{2-}) conducting ceramic as a solid electrolyte and a catalytic metal oxide as a working electrode.
- Apply a constant current-bias (through the electrolyte) between the working electrode and an "inert" counter electrode.
- Correlate the NO_x concentration with the potential associated with the applied current-bias.
- Optimize sensor performance by identifying and resolving materials science issues associated with sensitivity, response speed, cross-sensitivity, and stability

Accomplishments

- Submitted a patent application and conference abstract on the current-biased NO_x sensing technique.
- Published one journal article and one conference proceeding on related potentiometric NO_x sensor techniques.
- Identified electrode materials exhibiting ~90 mV response to 500 ppm NO at 650ºC with a 90% response time of t_{90} (baseline to 90% of equilibrium value) ~1.25 s.
- Sent a first-generation laboratory prototype of the current-biased NO sensor to Ford Research Center for sensitivity/selectivity testing (data presented in this report).
- Began cross-sensitivity testing for NO_2, O_2, H_2O, CO, CO_2, and NH_3.

Future Direction

- Continue to explore materials issues related to sensitivity and stability.
- Investigate sensing mechanism using electrochemical and analytical techniques.
- Evaluate microstructural evolution during sensor aging.
- Evaluate cross-sensitivity to important redox gases.
- Demonstrate the commercialization potential of the current-biased sensor technique.
- Transfer the technology to a commercial entity.

Introduction

New emissions regulations will increase the need for compact, inexpensive sensors for monitoring and control of automotive exhaust gas pollutants. Species of interest include hydrocarbons, carbon monoxide, and NO_x. The most promising NO sensors for exhaust gas monitoring are based on ionically conducting solid state electrochemical devices.[1,2] These devices typically consist of a solid ceramic electrolyte onto which two or more metal or metal-oxide electrodes are deposited, and they can be operated in either potentiometric or amperometric modes. Significant progress has been made toward the development of deployable sensors using yttria-stabilized zirconia (YSZ) as the electrolyte and catalytically active metal oxides as the sensing electrodes.[3] However, improvements are still needed in sensitivity, response time, reliability, and cross-sensitivity. The current work is directed toward the development of fast, high-sensitivity electrochemical NO_x sensors for automotive diesel applications.

A NO_x sensor with fast response time and high sensitivity to NO at 650ºC has been developed. The sensor is based on a novel current-biased mode of operation where a fixed current is applied between the sensing and counter electrodes and the resultant potential is measured. This method is distinctly different from conventional amperometric sensor technology. The target operating parameters for the proposed sensor (based on discussion with industry collaborators) are sensitivity to the total NO_x content in the range of 1 to 1000 ppm, operating temperature of >600°C, and a response time of 1 s.

Approach

The proposed approach is to develop a sensor using catalytic metal oxide electrodes on a solid ionic conductor electrolyte. Similar technology has been widely investigated for various gas sensing applications and has been successfully developed for use in exhaust gas oxygen sensors. The current effort approaches the problem by the application of novel materials and fabrication processes designed to optimize electrode microstructures. In addition, a novel mode of operation has been identified that yields enhanced NO response sensitivity and speed.

Sensors are prepared by spray deposition of metal oxide working electrodes onto dense YSZ electrolyte substrates, followed by sintering at 900–1000°C. Working electrodes are composed of nanocrystalline n-type semiconducting oxides, usually tin-doped indium oxide (ITO), promoted with a small addition of Rh metal. Counter electrodes are composed of platinum or PdAg applied using screen printing paste. NO_x sensing experiments are performed in a quartz tube inside a furnace using a standard gas handling apparatus. All tests were performed in the temperature range of 600–700°C.

Sensors are typically first evaluated by the generation of current–voltage (I-V) curves in

various atmospheres. These curves yield the current (I) as a function of applied voltage (V). The measured current is directly related to the amount of oxygen being "pumped" through the electrolyte by the reaction

$$\frac{1}{2}O_2 + V_O + 2e^- = O^{2-} \quad (1)$$

where V_O represents an oxygen vacancy and O^{2-} represents an oxide ion in the electrolyte lattice. Because all tests are performed in high O_2 (~10%) and low NO_x (≤ 500ppm) concentrations, changes in the I-V behavior indicate relative changes in the reaction kinetics upon a change in the gas composition. Once the I-V behavior is determined, the operating bias condition can be selected based on the desired NO and NO_2 sensitivities. Sensor testing under a constant current bias is then performed to determine the sensitivity and stability characteristics of the sensor.

Results

Figure 1 shows the I-V characteristic of the sensor when operated at 650°C in 10% oxygen and the balance nitrogen. Also shown are the data for 10% oxygen with 500 ppm NO or NO_2. It can be seen that the introduction of either NO_x species shifts the I-V behavior significantly, indicating changes in the electrochemical rate constants of the reactions occurring at the electrodes. The sensor can be biased galvanostatically (constant current) or potentiostatically (constant voltage). The introduction of 500 ppm NO, for example, is detected as a change in measured potential (galvanostatic mode) or current (potentiostatic mode), corresponding to shifting the I-V behavior from the 10% O_2 curve to the NO curve in Figure 1. Potentiostatic biasing is equivalent to the traditional amperometric mode of operation. However, we have postulated that there may be some performance benefits to operating in the current-biased, galvanostatic mode.

The data shown in Figure 2 were acquired during independent testing at Ford Research

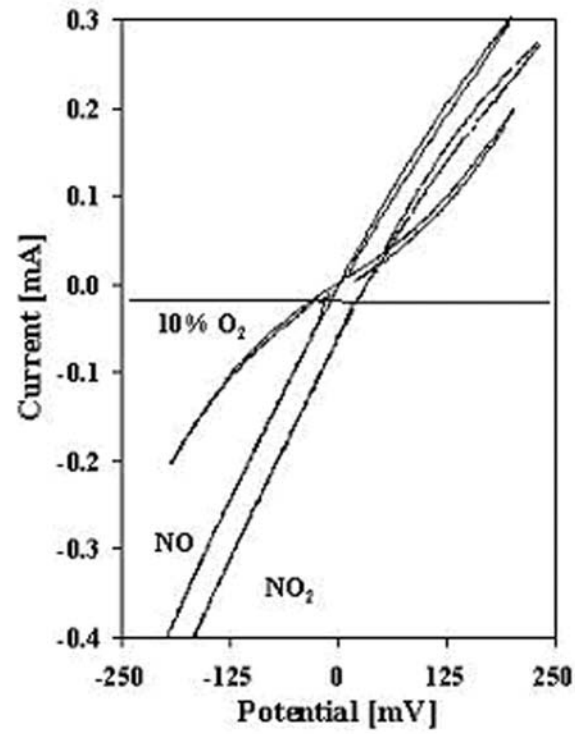

Figure 1. I-V characteristic in 10% O_2 and 10% O_2 plus 500 ppm NO or NO_2.

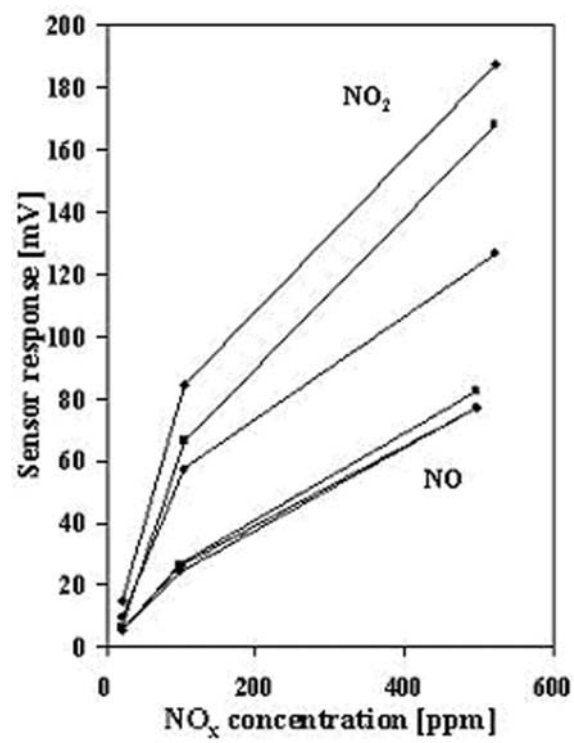

Figure 2. Sensor response to NO and NO_2 in 3(●), 10 (■), and 20% (♦) O_2.

Center.[4] As shown in Figure 2, when the sensor is negatively biased galvanostatically, the measured potential (response) is positive for both NO and NO_2. In comparison, traditional electrochemical potentiometric sensors have competing (opposite sign) responses to NO and NO_2. That the NO and NO_2 have the same sign response may suggest the possibility that both species are reduced during the negative bias, or possibly that the NO is being converted (non-electrochemically) to NO_2, which is then detected electrochemically. It is interesting to note that the effect of O_2 concentration is much more pronounced for NO_2 sensing than for NO.

Figure 3 shows the fast response of the sensor to 500 ppm NO and NO_2. The sampling interval in the figure is 0.25 s. Thus the 90% turn-on and turn-off times are ~1.25 and 2.5 s, respectively, for the NO response.

This fast response is attributed to the enhancement of the electrode kinetics caused by the biasing current. Ongoing investigations are being performed to elucidate the sensing mechanism. It has been observed during testing that there is a tendency for the sensor baseline to drift over time (~1-5 mV/hour). This drift is probably attributable to coarsening of the electrode microstructure during testing. Future efforts will involve identifying the mechanism for the baseline drift and evaluating means for stabilizing this effect. Possible techniques for accomplishing these tasks are modifying the electrode microstructure (for example, by incorporation of a more refractory phase), intentional aging of the electrodes, or selection of alternate electrode materials.

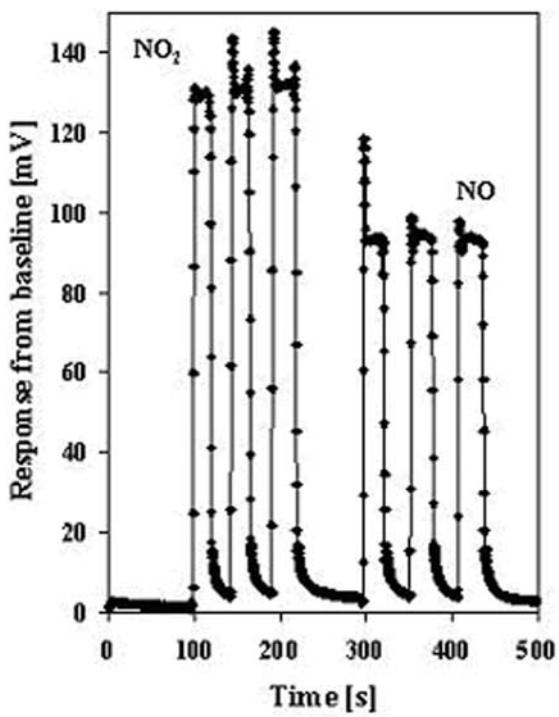

Figure 3. Sensor response vs time for 500 ppm NO and NO_2 in 10% O_2.

Conclusions

A novel current-biased mode of operation has been developed for NO_x sensing in automotive diesel exhaust. Electrode materials have been identified that provide excellent sensitivity and response time for sensing NO at 650°C in 10% O_2. This technique has generated significant interest from the automotive industry. Sensor stability and cross-sensitivity will be further addressed in future efforts. Long-term dynamometer testing is to be performed by Ford, and planning for ultimate technology transfer to a commercial entity has been initiated.

References

1. F. Menil, V. Coillard, and C. Lucat, "Critical Review of Nitrogen Monoxide Sensors for Exhaust Gases of Lean-Burn Engines," *Sensors and Actuators B*, **67**, 1–23 (2000).

2. N. Miura, G. Lu, and N. Yamazoe, "Progress in Mixed-Potential Type Devices Based on Solid Electrolyte for Sensing Redox Gases," *Solid State Ionics*, **136–137**, 533–542 (2000).

3. T. Ono, M. Hasei, A. Kunimoto, T. Yamamoto, and A. Noda, "Performance of the NO_x Sensor Based on Mixed Potential for Automobiles in Exhaust Gases," *JSAE Rev.*, **22**, 49–55 (2001).

4. Rick Soltis and Dave Kubinski, Ford Research Center, Dearborn, Michigan.

FY 2003 Publications/Presentations

L. P. Martin, Q. Pham, and R. S. Glass, "Effect of Cr_2O_3 Electrode Morphology on the NO Response of a Stabilized Zirconia Sensor," accepted for publication in *Sensors and Actuators B* (May 2003).

L. P. Martin, Q. Pham, and R. S. Glass, "Electrochemical NO_x Sensors for Automotive Diesel Exhaust," presented at the 2002 Materials Research Society Fall Meeting, Boston, Massachusetts, December 2–7, 2002. A paper with the same title was accepted for publication in the *Proceedings of the 2002 Materials Research Society Fall Meeting*, (in press, 2003).

L. P. Martin, D. Kubinski, R. Soltis, J. Visser, M. Parsons and R. S. Glass, "A Current-Biased NO_x Sensor for Automotive Diesel Exhaust," submitted for presentation at The 204th Meeting of The Electrochemical Society, Orlando, Florida, October 12–17, 2003.

L. P. Martin, D. Kubinski, R. Soltis, J. Visser, M. Parsons and R. S. Glass, "Galvanostatic NO_x Sensor Based on Yttria-Stabilized Zirconia and a Metal Oxide Working Electrode," submitted to *Solid State Ionics* (August 2003).

Patents

Patent application: L. P. Martin and A.-Q. Pham, "Current-Biased Potentiometric NO_x Sensor for Vehicle Emissions," LLNL Docket #: IL-11022, submitted April 2003.

APPENDIX A: ACRONYMS AND ABBREVIATIONS

AHE	aerodynamic heat exchanger
ANL	Argonne National Laboratory
ASTM	American Society for Testing and Materials
CIDI	compression-ignition direct-injection
CO	carbon monoxide
CRADA	cooperative research and development agreement
DF	dissipation factor
DOE	U.S. Department of Energy
DPF	diesel particulate filter
E	elastic modulus
EDM	electrodischarge machining
EDX	energy-dispersive X-ray spectroscopy
E/E	Electrical and Electronics
EGR	exhaust gas recirculation
EN	electroless nickel
EPA	Environmental Protection Agency
F	fluorine
FTP	Federal Test Protocol
GGFD	ground graphitized foam dust
GM	General Motors
GTRI	Georgia Tech Research Institute
H	hardness
HA-ADF	high-angle annular dark-field
H^+	hydrogen ion
H_2	hydrogen gas
HDI	high-density infrared
HEPA	high-efficiency particulate air (filter)
IC	internal combustion
ICC	integrated circuit chip
ICS	Industrial Ceramic Solutions
ID	internal diameter
LANL	Los Alamos National Laboratory
L/D	length-to-diameter
MEA	membrane electrode assembly
MLCC	multi-layer ceramic composite
MPM	mechanical properties microprobe
MQI	Magnequench International

MRE	mixed rare earth
MW-DPF	microwave-regenerated diesel particular filter
ND	neodymium
NEP	National Energy Policy
NFC	near-frictionless carbon
NIST	National Institute for Standards and Testing
nm	nanometer, 10^{-9} meters
NO	nitrogen oxide
NO_x	oxides of nitrogen
NSA	National Security Agency
NTP	nonthermal plasma
OAAT	Office of Advanced Automotive Technologies
OEM	original equipment manufacturer
OHVT	Office of Heavy Vehicle Technologies
OM	optical microscope
ORNL	Oak Ridge National Laboratory
OTT	Office of Transportation Technologies
PECS	passive evaporative cooling system
PEM	polymer electrolyte membrane
PEMFC	polymer electrolyte membrane fuel cell
Pd	palladium
PM	permanent magnet
PNGV	Partnership for a New Generation of Vehicles
PNNL	Pacific Northwest National Laboratory
POEM	porous oxide electrolyte membrane
PPS	polyphenylene sulfide
Pt	platinum
PVD	physical vapor deposition
PVOH	hydroxylated polystyrene
PVP	hydroxylated polystyrene
R&D	research and development
RE	rare earth
S	sulfur
SAE	Society of Automotive Engineers
SEM	scanning electron microscope
SHE	standard hydrogen electrode
SNL	Sandia National Laboratories
SO_3^{2-}	sulfonate group
STEM	scanning transmission electron microscope
T	Tesla
TEGDE	tetraethylene glycol divinyl ether
TEM	transmission electron microscope
TiN	titanium nitride
TiC	titanium carbide
TIVM	toroidal intersecting vane machine

WC	tungsten carbide
XRD	X-ray diffraction
YSZ	yttria-stabilized zirconium
Z	characterized by a high atomic number